

## EARLY-TYPE HOST GALAXIES OF TYPE IA SUPERNOVAE. II. EVIDENCE FOR LUMINOSITY EVOLUTION IN SUPERNOVA COSMOLOGY

YIJUNG KANG,<sup>1</sup> YOUNG-WOOK LEE,<sup>1</sup> YOUNG-LO KIM,<sup>2,1</sup> CHUL CHUNG,<sup>1</sup> AND CHANG HEE REE<sup>3</sup>

<sup>1</sup>*Center for Galaxy Evolution Research & Department of Astronomy, Yonsei University, Seoul 03722, Republic of Korea*

<sup>2</sup>*Université de Lyon, F-69622, Lyon, France; Université de Lyon 1, Villeurbanne; CNRS/IN2P3, Institut de Physique Nucléaire de Lyon*

<sup>3</sup>*Korea Astronomy and Space Science Institute, Daejeon 34055, Republic of Korea*

(Received; Revised; Accepted November 23, 2019)

Submitted to ApJ

### ABSTRACT

The most direct and strongest evidence for the presence of dark energy is provided by the measurement of galaxy distances using type Ia supernovae (SNe Ia). This result is based on the assumption that the corrected brightness of SN Ia through the empirical standardization would not evolve with look-back time. Recent studies have shown, however, that the standardized brightness of SN Ia is correlated with host morphology, host mass, and local star formation rate, suggesting a possible correlation with stellar population property. In order to understand the origin of these correlations, we have continued our spectroscopic observations to cover most of the reported nearby early-type host galaxies. From high-quality (signal-to-noise ratio  $\sim 175$ ) spectra, we obtained the most direct and reliable estimates of population age and metallicity for these host

galaxies. We find a significant correlation between SN luminosity (after the standardization) and stellar population age at a 99.5% confidence level. As such, this is the most direct and stringent test ever made for the luminosity evolution of SN Ia. Based on this result, we further show that the previously reported correlations with host morphology, host mass, and local star formation rate are most likely originated from the difference in population age. This indicates that the light-curve fitters used by the SNe Ia community are not quite capable of correcting for the population age effect, which would inevitably cause a serious systematic bias with look-back time. Notably, taken at face values, a significant fraction of the Hubble residual used in the discovery of the dark energy appears to be affected by the luminosity evolution. We argue, therefore, that this systematic bias must be considered in detail in SN cosmology before proceeding to the details of the dark energy.

*Keywords:* cosmology: observations — distance scale — dark energy — galaxies: elliptical and lenticular, cD — supernovae: general

## 1. INTRODUCTION

Despite the general consensus, the presence and nature of the dark energy are currently the most serious conundrum in astrophysics and cosmology. The distance measurements using type Ia supernovae (SNe Ia) for the galaxies at high redshift have provided the most direct evidence for the accelerating universe with dark energy (Riess et al. 1998; Schmidt et al. 1998; Perlmutter et al. 1999). In order to use the SNe Ia as a standard candle, however, the “standardization” is required because of a large spread in their intrinsic luminosity. This is fulfilled through the empirical procedures based on their light-curve shape and color (e.g., Phillips 1993; Riess et al. 1996; Perlmutter et al. 1997; Guy et al. 2007; Jha et al. 2007). In SN cosmology, it is further assumed that this standardized SN Ia brightness does not evolve with look-back time. However, in observational cosmology, there is always a possibility of the luminosity evolution of standard candle with redshift, as first pointed out by Tinsley (1968). Obviously, SN progenitors in host galaxies are getting younger with redshift, and

several investigators had some doubts on the assumption of no luminosity evolution in SN cosmology although they were not based on observational evidence (e.g., [Drell et al. 2000](#); [Ferramacho et al. 2009](#); [Linden et al. 2009](#); [Tutusaus et al. 2017, 2019](#)). According to the analysis by [Childress et al. \(2014\)](#), the difference in the mean age of SN progenitors between  $z = 0$  and 1.0 is predicted to be  $\sim 5.3$  Gyr (see also Section 4 below). It is therefore possible that SNe at high redshift are fainter (after the standardization) than the value expected from the model without the dark energy, not because of the dark energy, but mostly because of the luminosity evolution. Careful investigation of this possible systematic bias with redshift is particularly important because the dimming of SNe is only  $\sim 0.2$  mag ( $\sim 20\%$  in brightness) with respect to a cosmological model without dark energy ( $\Omega_M = 0.27$ ,  $\Omega_\Lambda = 0.00$ ; [Hicken et al. 2009](#)).

Nevertheless, to test the effect of luminosity evolution, in the discovery papers, [Riess et al. \(1998\)](#), [Schmidt et al. \(1998\)](#), and [Perlmutter et al. \(1999\)](#) only used morphological classification of host galaxies in the local universe as a proxy for stellar population age. Because of apparently very small difference in the standardized brightness between SNe Ia in the early-type and late-type host galaxies, they concluded that the luminosity evolution is negligible in SN cosmology. Later analysis based on a larger sample by [Hicken et al. \(2009\)](#), however, found a systematic difference of  $\sim 0.14$  mag between the very early- and very late-type galaxies (see also [Suzuki et al. 2012](#)). Recent investigations of host galaxies further found a correlation between the SN brightness<sup>1</sup> and host mass, suggesting that SNe Ia in less massive galaxies are  $\sim 0.1$  mag fainter than those in more massive galaxies ([Kelly et al. 2010](#); [Sullivan et al. 2010](#); [Childress et al. 2013](#); [Johansson et al. 2013](#)). More recent studies based on star formation rate (SFR) in host galaxies also showed that the SNe Ia in locally star-forming environments are fainter than those in locally passive environments ([Rigault et al. 2015](#); [Kim et al. 2018](#); [Rigault et al. 2018](#); [Roman et al. 2018](#); [Rose et al. 2019](#)). Since the host morphology, host mass, and the physics of star formation cannot directly affect SN luminosity, all of these correlations

<sup>1</sup> Throughout this paper, unless otherwise specified, by SN Ia brightness/luminosity, we are referring to the standardized brightness/luminosity after the light-curve shape and color corrections.

are probably not directly originated from these host properties, but more likely due to the age or metallicity of the SN Ia progenitor closely related to these properties.

In order to directly test this, 9 years ago, we have initiated the project YONSEI (YOnsei Nearby Supernovae Evolution Investigation). For this project, we have observed  $\sim 60$  target galaxies selected from the YONSEI SN catalog (Kim et al. 2019), covering most of the reported nearby ( $0.01 < z < 0.08$ ) early-type host galaxies. The standardized brightnesses of SNe Ia in these target galaxies were obtained from the light-curve fitters implemented in the SuperNova ANALysis software (SNANA; Kessler et al. 2009) package. Our target galaxies are restricted to the early-type galaxies because a reliable age dating is possible for them from the absorption-line dominated spectra, and their dust extinction is relatively negligible (see Gallagher et al. 2008 for the pioneering work). For each target galaxy, the absorption lines from very high quality (signal-to-noise ratio [S/N]  $\sim 175$ ) spectra have been used to determine population age, metallicity, and velocity dispersion by employing the population synthesis models. This is the well-established technique in the extragalactic community that can provide the best age dating for distant galaxies where the individual stars are not resolved (Faber et al. 1992; Worthey 1994; Worthey & Ottaviani 1997; Cardiel et al. 1998; Trager et al. 2000; Thomas et al. 2005; Graves et al. 2009; Thomas et al. 2010).

In Paper I of this series (Kang et al. 2016), based on 27 host galaxies, we reported that early-type host galaxies are also following the “downsizing” trend, the well-known correlation between the mass (velocity dispersion) and population age of non-host galaxies. This result suggested that stellar population age is mainly responsible for the correlation between host mass and standardized SN brightness, which, when confirmed, would imply that the luminosity evolution plays a major role in the systematic uncertainty of SN cosmology. Here, as the second paper of this series, we aim to directly confirm the possible luminosity evolution of SN Ia with population age. We have obtained spectra for 32 additional host galaxy sample which has been combined with the dataset previously reported in Paper I, securing a sufficient number of host galaxies required for the purpose of this paper. We have also revisited previously reported correlations of SN brightness with host morphology, host mass, and SFR, in order to compare them with our result based on population age.

## 2. OBSERVATIONS AND DATA ANALYSES

In Paper I, we reported spectroscopic observations made for the nearby early-type host galaxies at Las Campanas Observatory (LCO) 2.5-m telescope in the southern hemisphere. Here we have continued our observations at MMT 6.5-m telescope for the targets observable from the northern hemisphere. As in Paper I, our host galaxy sample is limited to nearby targets in the redshift range of  $0.01 < z < 0.08$  with  $11.69 < B < 18.4$  mag. We have selected only early-type galaxies (ETGs; E-S0) based on the morphological classification in the NASA Extragalactic Database (NED) or the HyperLeda database (Makarov et al. 2014).

The light-curve parameters for SNe occurred in host galaxies were extracted from the YONSEI SN catalog (Kim et al. 2019) which consistently combined the data from various surveys over a wide redshift range. This catalog contains the light-curve shape, color and extinction parameters, together with the values for the observed rest-frame peak apparent magnitude in  $B$ -band ( $m_B$ ) and the estimated distance ( $\mu_B$ ) calculated from two independent light-curve fitters, SALT 2.4 (Guy et al. 2007; Betoule et al. 2014) and MLCS2k2 (Jha et al. 2007). The best-fit cosmological parameters from this catalog are  $\Omega_M = 0.30$ ,  $H_0 = 70$ ,  $\alpha = 0.15$ ,  $\beta = 3.69$ , and  $M_B = -19.06$  mag for SALT2, assuming a flat  $\Lambda$ CDM model. From these parameters, the value for the Hubble residual (HR) is estimated, which is defined as the difference in distance modulus between that measured from SN Ia and that predicted from adopted cosmology ( $HR \equiv \mu_{SN} - \mu_{model}(z)$ ).<sup>2</sup> Since the purpose of this paper is to examine the systematic variation of SN luminosity with host property, the intrinsic dispersion ( $\sigma_{int}$ ) is set to 0, as generally adopted in SN host galaxy studies (e.g., D’Andrea et al. 2011; Gupta et al. 2011; Pan et al. 2014). In this paper, we only use the parameters derived from SALT2 because those from MLCS2k2 have higher intrinsic dispersion likely due to the lack of recent calibration (see Jones et al. 2015). The light curve parameters listed in the YONSEI catalog are in good agreements

<sup>2</sup> Here we have adopted the  $\Lambda$ CDM model ( $\Omega_M = 0.30$ ,  $\Omega_\Lambda = 0.70$ ) for the calculation of the Hubble residual. However, since we are dealing with only the nearby sample, almost identical values would be obtained even we had adopted other cosmological model.

with those obtained by other investigators. The readers are referred to [Kim et al. \(2019\)](#) for a more detailed description of this catalog.

Since the purpose of this paper is to investigate the correlation between SN brightness and global host property, additional target galaxies observed at MMT 6.5-m were selected for which SN light-curve parameters,  $m_B$ , and/or  $\mu_B$  are provided in YONSEI SN catalog. In addition, we only selected host galaxies in which SNe are located within 5 effective radius (as defined by [Cappellari et al. 2011](#)) so that the population property of SN progenitor would not be very different from the global property measured in the central region of each galaxy. Among the host galaxy sample of Paper I observed at LCO, 20 galaxies satisfy these criteria. A host galaxy of SN 2007ba, UGC 09798, was further excluded from our sample due to an extreme peculiarity of its SN (see [Hicken et al. 2009](#); [Burns et al. 2014](#); [Scalzo et al. 2019](#)). Table 1 lists the basic information of our total sample of host galaxies to be used in this paper, including 19 galaxies among those reported in Paper I. The SALT2 light-curve parameters of SNe Ia in our sample are listed in Table 2. For 32 host galaxies added in this paper, the digitized sky survey (DSS) images marked with SN Ia position are shown in Figure 1.

For the additional sample of host galaxies, observations have been carried out using the long-slit Blue Channel Spectrograph on MMT 6.5-m during the three observing runs in May 2014, January 2015, and December 2016. As listed in Table 1, the typical single exposure time for each galaxy was 600 - 1800 seconds depending on the target brightness and/or the sky condition. The settings for the slit position angle (PA) and for the calibration frames (dome flats, twilight sky flats, and HeNeAr arc lamp) are mostly identical to those described in Paper I. Table 3 lists an instrumental setup for our long-slit spectroscopy. Following the usual manner, we have observed standard stars for flux calibration, radial velocity correction, and telluric feature removal. To transform the measured indices to the Lick/IDS standard system, we have further observed 27 stars from the Lick library ([Worthey et al. 1994](#); [Worthey & Ottaviani 1997](#)). To check for the possible systematic offset between the measured indices from LCO and MMT, we have also revisited 11 early-type galaxies (5 host galaxies, 6 non-host galaxies) covered in Paper I. In addition to this, 4 more non-host galaxy spectra were taken for the consistency check with previous studies in the literature.

For the data reduction, we followed the same procedures described in Paper I - the IRAF<sup>3</sup> based routines for the basic preprocessing and for the long-slit spectroscopic analysis. In order to obtain reliable stellar population age and metallicity, the typical S/N of our target galaxies was aimed to be unusually high,  $\sim 175$  per pixel (at  $5000 \text{ \AA}$ ), and thus, even the faintest galaxies in our sample have S/N of more than  $\sim 65$ . From our fully calibrated spectra, possible contaminations by weak emission lines, if any, were removed using the GANDALF (Gas AND Absorption Line Fitting; Sarzi et al. 2006) package based on the pPXF (Penalized Pixel-Fitting; Cappellari & Emsellem 2004) method. Most of the parameters and setups for this procedure were following the descriptions in Paper I. As an example, Figure 2 compares the absorption line features for NGC 2258, before and after the emission correction. We measured the Lick indices for host galaxies using *lick\_ew* procedure in *EZ\_ages* package (Graves & Schiavon 2008) from the emission cleaned spectra, with a correction for the velocity dispersion broadening. We refer the reader to Paper I for the details of the procedures adopted in our data reduction. The measured indices were then transformed to the Lick/IDS standard system using the standard stars in Worthey et al. (1994) and Worthey & Ottaviani (1997). Figure 3 shows the mean offset of each index between our MMT observations and the Lick/IDS database, which was used for the zero-point correction. As the last step, we have combined the two datasets from our observations made at LCO and MMT. For this, the Lick indices of 11 galaxies common in both datasets were compared as shown in Figure 4, from which the measured values of MMT spectra were shifted to the LCO system. In Figure 5, our measured indices for non-host early-type galaxies observed at MMT are compared with those reported in the literature (Trager et al. 1998, 2000; Kuntschner et al. 2001, 2010; Denicoló et al. 2005; Sánchez-Blázquez et al. 2006). Similarly to the result reported in Paper I, our measurements are consistent with previous measurements to within  $-0.03$ ,  $-0.12$ ,  $0.070$ ,  $0.20 \text{ \AA}$ , and  $\sim 10 \text{ km/s}$  for  $H\beta$ , Fe5270, Fe5335, Mg *b*, and  $\sigma_v$ , respectively. These small offsets are comparable to those generally shown in other studies and are expected from the differences in the adopted aperture size, instruments used, and/or the procedures employed for

<sup>3</sup> IRAF is distributed by the National Optical Astronomy Observatory, which is operated by the Association of Universities for Research in Astronomy (AURA) under cooperative agreement with the National Science Foundation.

the emission correction. The fully-corrected Lick indices ( $H\beta$ , Fe5270, Fe5335, and  $Mg\ b$ ), together with the measured velocity dispersion ( $\sigma_v$ ), for our total sample are listed in Table 4.

### 3. CORRELATION BETWEEN POPULATION AGE AND HUBBLE RESIDUAL OF SN IA

With the measured Lick indices,  $H\beta$ ,  $Mg\ b$ , and  $\langle Fe \rangle^4$ , here we determine the luminosity-weighted age and metallicity of stellar population composing the central region of host galaxies. For this, we adopt three different evolutionary population synthesis (EPS) models from Chung et al. (2013, Yonsei Evolutionary Population Synthesis, hereafter YEPS), Thomas et al. (2011, hereafter TMJ11), and Schiavon (2007, hereafter S07). As described in detail in Paper I, age and metallicity ( $[M/H]$ ) are simultaneously determined from these models on the  $\langle Fe \rangle$ - $H\beta$  model grid. Figure 6 compares the measured  $\langle Fe \rangle$  and  $H\beta$  indices of our host galaxy sample with each of these EPS models for  $[\alpha/Fe]=0.3$ . Table 5 lists the derived values for population age and  $[M/H]$ , together with their errors, from YEPS, TMJ11, and S07 models, respectively. In Figure 7, two example spectra for relatively young and old host galaxies are compared, where one can see a difference in the depth of  $H\beta$  line between these two galaxies.

For the purpose of this paper, we need to select only genuine early-type galaxies with absorption-dominated spectra from passive environments without ongoing star formation. However, some galaxies in our sample, although they are morphologically classified as early-type galaxies, show strong emission lines on their spectra, indicating they have more characteristics of late-type environments than early-type systems. They appear as if they have very young ages ( $<2.5$  Gyr) after strong emission line correction. According to Thomas et al. (2010), such galaxies apparently younger than 2.5 Gyr in terms of luminosity-weighted age have most likely been “rejuvenated” by recent episode of star formation (see also Yi et al. 2005; Shapiro et al. 2010). For these rejuvenated galaxies, as demonstrated by many investigators (see, e.g., Greggio 1997; Nolan et al. 2007; Serra & Trager 2007), only a few percent of very young stellar population can significantly affect the luminosity-weighted age. Therefore, the majority ( $>90\%$ ) of stellar populations in these galaxies can still be markedly older

<sup>4</sup>  $\langle Fe \rangle \equiv (Fe5270 + Fe5353)/2$



than the determined mean age. In our sample, six galaxies, including NGC 5018 (Nolan et al. 2007; Spavone et al. 2018), are classified as such rejuvenated galaxies. They also show star-forming rings, gas lanes, and/or disturbed features on their DSS image (see Figure 1), all indicating features of recent episodes of merger-induced starburst. Additional IFU observations and analyses would be required for these galaxies to dissect into young and old components, which, however, is still a very challenging task (see, e.g., Gu erou et al. 2016; Zibetti et al. 2019). For this reason, here we have excluded these rejuvenated galaxies from further analyses because their mean ages are seriously underestimated or highly uncertain. In addition to these galaxies, some of our host galaxies can still contain a small fraction of young stellar component. In order to check this, when available, we have examined the level of young star contamination in our host sample by using the *NUV*-, *r*-, and *W3*-band images from GALEX (Martin et al. 2005), SDSS (Abolfathi et al. 2018) or DESI Legacy Imaging Surveys (Dey et al. 2019), and unWISE (Lang 2014) databases. We find that three galaxies (hosts of SN 2002G, SN 2007cp, and SN 2007R) have very large excess emissions both in *NUV* and *W3*, clearly separated from other host galaxies (see Figure 8), indicating a significant contamination from ongoing or recent star formation. Along with the rejuvenated galaxies, these UV/IR excess galaxies are further excluded from our final analyses as their derived ages are highly uncertain.

Following our Paper I, in Figure 9, we first compare the velocity dispersion (a proxy of galaxy mass) with population age and metallicity for our final sample of host galaxies. As in our previous analysis, we perform the linear fitting using the Markov Chain Monte Carlo (MCMC) analysis implemented in the LINMIX package (Kelly 2007). Host mass and population age show a strong correlation, which corresponds to >99.9% probability for the non-zero slope in all cases of adopted EPS model <sup>5</sup>. This is consistent with the result reported in Paper I, but the present result is based on a larger sample. In contrast, the metallicity shows no meaningful correlation with velocity dispersion (see Figure 10).

<sup>5</sup> To estimate the confidence level, we fit the posterior distribution of slopes with a Gaussian function, and computed the standard deviation of the slopes and computed how many sigma the mean is away from zero, then converted that to a probability.

It is well-established that SN light-curve parameters (decline rate or stretch factor) are correlated with peak luminosity before standardization (Phillips 1993; Riess et al. 1999; Hamuy et al. 2000; Howell 2001; Sullivan et al. 2006). Previous studies based on indirect or secondary age indicators (spectral energy distribution [SED], SFR, morphology) for host galaxies (e.g., Howell et al. 2009; Neill et al. 2009; Johansson et al. 2013; Rose et al. 2019) also found a strong correlation between the stretch factor and population age, in the sense that younger population tends to host intrinsically brighter SN Ia. In Figure 11, we plot SALT2 stretch factor ( $X_1$ ) with population age for our host galaxy sample, which shows qualitatively consistent correlation with previous studies, although the statistical significance is lower ( $\sim 86\%$  confidence level). This is probably because our result is based only on ETGs with relatively narrow spans of age (2.5 Gyr - 10.5 Gyr with YEPS) and the light-curve stretch value.

As described above, the SN brightness after light-curve shape and color corrections, instead of the intrinsic luminosity, is being used in SN cosmology, and therefore, it is crucial to see the correlation between stellar population age and standardized SN brightness. Figure 12 shows a correlation of stellar population age with the Hubble residual calculated from standardized SN Ia brightness. Note that, on this diagram, a positive value of Hubble residual indicates a relatively fainter SN Ia after the standardization, while a negative value corresponds to a brighter SN Ia. Interestingly, at first glance, no sample galaxy appears to be located in the upper-right regime of the diagram, which would imply a correlation between age and standardized SN brightness. Rose et al. (2019) also noted a similar distribution from their study with SED-based age dating. In Figure 13, we perform the MCMC analysis with our final sample (excluding rejuvenated and UV/IR excess galaxies). We find that the population age is correlated with the standardized brightness (Hubble residual) at a  $\sim 99.5\%$  confidence level. Note that our result is insensitive to the choice of population synthesis model, as they all show qualitatively consistent results in the sense that SN Ia in younger host tends to be fainter than that in older host. It is important to note, from the comparison of Figure 13 with Figure 12, that contamination of non-genuine early-type galaxies (rejuvenated and UV/IR excess galaxies) would make the correlation apparently weaker. Therefore, careful selection of only normal

early-type galaxy sample is important for this study. In that respect, it is reassuring to see that the correlation is getting stronger when the contamination from non-genuine early-type galaxies is properly taken into account. For the quantitative analysis in the following section, we will adopt the result from YEPS because it is based on the more realistic treatment of Helium burning stage in the stellar evolution modeling and is well-calibrated to the color magnitude diagrams, integrated colors, and absorption indices of globular clusters in the Milky Way and nearby galaxies (Lee et al. 2005; Chung et al. 2013, 2017; Joo & Lee 2013; Kim et al. 2013). It is also producing ages for oldest host galaxies which are not inconsistent with the age of the universe. Unlike population age, we find no significant correlation between host metallicity and Hubble residual (see Figure 14). In Table 6, we summarize the results of our statistical analyses.

#### 4. DISCUSSION

In this paper, we have made a critical test on the possibility of the luminosity evolution in SN cosmology by investigating the correlation between SN Ia brightness and stellar population age of early-type host galaxies. Based on the most reliable age dating from high-quality absorption-dominated spectra and well-established stellar population models, we found a significant correlation between standardized SN brightness and stellar population age at  $\sim 99.5\%$  confidence level. As such, this is the most direct and stringent test ever made for the luminosity evolution of SN Ia. This result makes it possible to shed new light on the origin of the previously reported correlations of SN Ia luminosity with host morphology, host mass, and local SFR. Below we discuss how our result is related and could be accommodated with these previous studies.

As briefly described in Section 1, the very first test for the possible luminosity evolution of SN Ia, after the light-curve corrections, was to use the host galaxy morphology as a proxy for stellar population age (Riess et al. 1998; Schmidt et al. 1998; Perlmutter et al. 1999). Although this possibility was initially ruled out from no apparent dependence of SN luminosity with a limited sample of host morphologies, more recent analysis with a larger sample shows a different result (Hicken et al. 2009). This latter study, where the effect of dust extinction was carefully corrected, reported that SNe occurred within the late-type (Scd-Irr) galaxies are  $\sim 0.14$  mag fainter than those hosted by the

early-type (E-S0) galaxies (see also [Suzuki et al. 2012](#) for a similar result). If their result is interpreted as originally intended in the discovery papers, this dependence must indicate the difference in stellar population age. That the stellar populations in late-type galaxies are younger, in the mean, than those in early-type galaxies is a well-established result in extragalactic studies. According to the recent studies based on high-quality spectroscopic data (see, e.g., Figure 6 of [Scott et al. 2017](#)), stellar populations in late-type (Scd/Sd) galaxies are in the mean  $\sim 4$  Gyr younger than those in early-type (E/S0) galaxies. The most plausible interpretation of the result of [Hicken et al. \(2009\)](#) is therefore that a SN Ia occurred at a younger host galaxy is fainter than that found in an older host galaxy ( $\sim 0.14$  mag/4 Gyr). It is interesting to see that this conversion to age effect is not only consistent with but also quantitatively comparable to our result from population age and SN Ia luminosity (see Figure 13 and Table 6).

The mass of a host galaxy was then adopted as a proxy for population properties in many host galaxy studies. Among these, careful investigations by [Sullivan et al. \(2010\)](#) and [Kelly et al. \(2010\)](#) have established that SNe Ia in less massive galaxies (by a factor of 10) are  $\sim 0.08$  mag fainter than those in more massive galaxies. Since the mass of a galaxy cannot directly affect the brightness of SN Ia occurred in a host, while the mass of a progenitor would have a direct impact on the intrinsic luminosity of SN Ia ([Umeda et al. 1999](#); [Howell et al. 2009](#); [Johansson et al. 2013](#)), this correlation must be originated from either population age or metallicity. Among non-host galaxies, there is a well-established correlation between galaxy mass and stellar population age ([Thomas et al. 2005](#); [Neistein et al. 2006](#)). We have shown in Paper I that host galaxies are also following this “downsizing” trend with no apparent dependence on metallicity. The same result based on a larger sample in Figure 9 shows that less massive host galaxies (by a factor of 10) are  $\sim 2$  Gyr younger (based on YEPS) than more massive galaxies. Therefore, the apparent correlation with host mass is, again, most likely due to the effect of stellar population age ( $\sim 0.08$  mag/2 Gyr), which is also consistent with the results from our direct age dating and from the morphological classification described above.

More recent studies based on spectroscopy measured a local SFR in the vicinity of the site where SN Ia arose in a host galaxy. The local SFR can be readily and reliably obtained from the emission

lines which are observed in a significant fraction of host galaxies (Rigault et al. 2013, 2015, 2018; Galbany et al. 2014). Among these studies, Rigault et al. (2018) showed that SNe Ia in locally star-forming environments (higher local SFR) are  $\sim 0.16$  mag fainter than those in locally passive environments (lower local SFR), after the conventional light-curve corrections. Since the physics involved in SFR would not change the SN luminosity directly, this correlation is also most likely due to the stellar population age. Rigault et al. (2018) also suggested that this difference is originated from the different fraction of young to old stars between the star-forming and the passive environments. In this respect, more detailed analysis for the typical SN progenitor ages can be performed for the two environments. For the locally star-forming environment, firstly, we adopt the stellar population age from Galbany et al. (2014) which was derived from the spectral fitting technique with the spectral synthesis code STARLIGHT (Cid Fernandes et al. 2005). Out of 36 host galaxies with normal SN Ia in their sample, 10 galaxies belong to the locally star-forming group ( $\Sigma SFR_{SN} > 10^{-2}$  or  $\log M_{\star} < 10$ ) as defined by Rigault et al. (2018), and for them we obtain the mean age of  $\sim 0.6$  Gyr. A similar quantity is also derived by convolving the SN Ia delay time distribution (DTD) with a local star formation history (SFH) as demonstrated by Childress et al. (2014). For this, we employ a SFH of the Milky Way disk (the solar neighborhood) from the analyses of Bernard (2018) as a representative for the star-forming environment. When this SFH is coupled with a DTD of SN Ia suggested by Childress et al. (2014), the peak of the SN progenitor age distribution is also found at  $\sim 0.5$  Gyr. As to the locally passive environment ( $\Sigma SFR_{SN} < 10^{-2}$  and  $\log M_{\star} > 10$ ), 19 galaxies in Galbany et al. (2014) belong to these criteria, and for this group, we obtain the mean age of  $\sim 2.3$  Gyr. Six galaxies in our sample (Table 1) are in common with the list of host galaxies in Childress et al. (2013), and for these early-type galaxies (locally passive environments), the mean population age from our study is  $\sim 3.8$  Gyr. By taking the mean value of the two analyses for each environment, we adopt  $\sim 0.6$  Gyr as a typical age of the stellar population in locally star-forming environments and  $\sim 3.1$  Gyr for that in locally passive environments. Therefore, the 0.16 mag difference between the locally star-forming and locally passive environments is most likely due to a  $\sim 2.5$  Gyr difference in stellar population age. This difference is still comparable with the result we obtained from our early-type host galaxies.

Table 7 summarizes the results from these analyses compared with the slope ( $\Delta\text{HR}/\Delta\text{age}$ ) derived from our direct age dating. The last column lists the converted value from each of the host properties to the age difference. Note that, when interpreted as a population age effect, these four different and independent approaches are all pointing to the same direction — SNe Ia in younger environments are fainter than those in older environments, after the standardization of SN brightness. It is important to note that all of the three well-established correlations between the SN brightness and host property are not only qualitatively consistent but also quantitatively comparable to our result based on population age. Furthermore, all of these host properties (morphology, mass, and local SFR) are closely interrelated as described above. Based on these, we believe that the correlation with population age is most likely the original correlation that drove the previously reported correlations with host properties. This appears to be the only plausible interpretation that can explain all of these correlations (including our own) simultaneously.

Our result, together with the age interpretation of the previously reported correlations, inevitably suggests the SN luminosity evolution with redshift. This is because, as is well-known, host galaxies at  $z \sim 0.0$  consist of both young and old stellar populations whereas those at high redshift only consist of young population. Previous studies based on host mass and local SFR only considered the redshift evolution of these quantities, instead of population age, and therefore the applied corrections on the SN luminosity with redshift were negligible. In order to estimate the effect of luminosity evolution based on our result, we first derive the SN Ia progenitor age distribution as a function of redshift following the methodology in [Childress et al. \(2014\)](#). The SN Ia progenitor age distribution at epoch  $t_0$  of a given redshift  $z$  of the SN exploding from a progenitor system of age  $\tau$ ,  $P(\tau; t_0)$ , is derived by convolving DTD  $\phi(\tau)$  of SN Ia with cosmic SFH  $\psi(t_0 - \tau)$  in the form of  $P(\tau; t_0) = \phi(\tau)\psi(t_0 - \tau)$  (see Figure 3 of [Childress et al. 2014](#)). Specifically, we use a smooth function for DTD suggested by [Childress et al. \(2014\)](#):

$$\phi(t) \propto \frac{(t/t_p)^\alpha}{(t/t_p)^{\alpha-s} + 1}, \quad (1)$$

where the prompt time-scale ( $t_p$ ) is adopted to be 0.3 Gyr and the power law slope ( $s$ ) is set to -1 with  $\alpha = 20$ . As for the cosmic SFH, we also adopt an empirical function derived by Behroozi et al. (2013) from the collected cosmic SFR (CSFR) data:

$$CSFR(z) = \frac{C}{10^{A(z-z_0)} + 10^{B(z-z_0)}}, \quad (2)$$

where constants  $A = -0.997$ ,  $B = 0.241$ ,  $C = 0.180$ , and  $z_0 = 1.243$  are as given in Table 6 of their paper. The calculated SN Ia progenitor age distribution is shown in Figure 15, following the color-coding of Childress et al. (2014). Note that the SN progenitor age distribution at  $z = 0.0$  is strongly bimodal with two peaks at  $\sim 9.4$  Gyr and  $\sim 0.4$  Gyr, which would correspond to the “delayed” and “prompt” components of SNe Ia (Sullivan et al. 2006; Childress et al. 2014), whereas the distribution at  $z > 0.5$  has only a single peak which converges to the peak value of the DTD at  $\sim 0.4$  Gyr. As discussed below, this is important stellar astrophysics that must be considered in detail in SN cosmology. In the lower panels, the median age of the distribution and the  $\Delta$ age with respect to  $z = 0.0$  are also plotted as a function of redshift. According to this, the median ages of SN progenitors are  $\sim 6.54$  Gyr at  $z = 0.0$  and  $\sim 1.25$  Gyr at  $z = 1.0$ , so the difference in population age between these two epochs is  $\sim 5.3$  Gyr. It is important to note that the  $\Delta$ age at high redshift is converging to  $\sim 5.3$  Gyr because the median value of the SN Ia progenitor age distribution is asymptotically approaching to the peak value of  $\sim 0.4$  Gyr beyond  $z \sim 0.7$ . As discussed in Childress et al. (2014), the  $\Delta$ age is not strongly affected by the choice of  $t_p$  and  $s$  for the SN Ia DTD.

In the last column of Table 7, we list an estimated amount of the luminosity evolution that corresponds to this age difference for each of the four different studies. The mean value of these quantities is  $\sim 0.25$  mag/5.3 Gyr. Over the same redshift range, the observed dimming of SN brightness in the Hubble diagram is roughly comparable to this value (see, e.g., Riess et al. 1998; Hicken et al. 2009). Figure 16 shows our prediction of the SN Ia luminosity evolution in the residual Hubble diagram. The red line shows the evolution curve based only on the age dating of early-type host galaxies,

while the green line is produced using the mean value of  $\Delta\text{HR}/\Delta\text{age}$  from the four different studies on host properties. Since the purpose of this paper is to quantify the SN luminosity evolution with redshift and to illustrate the level of its significance, following [Hicken et al. \(2009; their Figure 1\)](#) and [Riess et al. \(1998\)](#), the Hubble residuals in this diagram are calculated with respect to the cosmological model without dark energy ( $\Omega_M = 0.27$ ,  $\Omega_\Lambda = 0.00$ ). The SN data over-plotted are adopted from the binned values of [Betoule et al. \(2014; their Table F.1\)](#). Importantly, our evolution curve is substantially different from that simply proportional to redshift (see the yellow curve in [Figure 16](#)) as employed by [Riess et al. \(2004; see also Drell et al. 2000\)](#). This is because the luminosity evolution of SN Ia, which is dictated by stellar astrophysics, is not linearly proportional to redshift, but determined by the SN Ia progenitor age distribution whose median value converges to  $\sim 0.4$  Gyr beyond  $z \sim 0.7$ . Therefore, the shape of our evolution curve appears almost identical to that in redshift vs.  $\Delta\text{age}$  diagram in [Figure 15](#).

Note that we implicitly assume a linear correlation between population age and Hubble residual over the full redshift range in [Figure 16](#) for all SNe Ia used in cosmological sample. This assumption could be somewhat uncertain at high redshift, because our SN Ia sample has been restricted predominantly to those with low stretch factor ( $X_1 \lesssim 0.0$ ) preferentially discovered in early-type galaxies. While a substantial fraction (32%) of SNe Ia still belongs to this category ( $X_1 < 0.0$ ) even at  $z > 0.5$  (see [Figure 3 of Kim et al. 2019](#)), assuming that all SNe Ia in cosmological sample will follow our relation between population age and SN Ia luminosity would require further justification. If high stretch ( $X_1 > 0.0$ ) SNe Ia in the cosmological sample somehow do not follow the same luminosity evolution, we would see a sizable difference in the Hubble residual between the low and high stretch sub-samples. For the SNe Ia with diverse stretch values ( $-3 < X_1 < 2$ ), the analysis by [Scolnic & Kessler \(2016; their Figure 3\)](#), however, shows only negligible difference in HR compared to the amount of the luminosity evolution suggested in this paper ( $\Delta\text{HR} \sim 0.2$  mag at  $z > 0.5$ ), indicating that the luminosity evolution would have affected more or less equally to the cosmological sample regardless of the stretch factor. Only very high stretch ( $X_1 > 2$ ) sub-sample of [Scolnic & Kessler \(2016\)](#) shows some meaningful difference, but it comprises only  $\sim 1.2\%$  of the total sample. [Sullivan et al. \(2011;](#)



their Table 8) also shows that the derived cosmological parameters are consistent between the low and high stretch SN Ia sub-samples. Furthermore, a similar result we obtained for the luminosity evolution from the four different host properties in Table 7, which involves both low and high stretch SNe Ia, would also imply that our assumption in the cosmological analysis is not grossly incorrect. In Figure 17,  $1\sigma$  significance interval of our evolution curve is added which is obtained from the regression fit of Figure 13. Strikingly, the comparison of our evolution curves with SN data in Figures 16 and 17 shows that the luminosity evolution can mimic a significant fraction of the Hubble residual (the difference in standardized SN brightness) used in the discovery and inference of the dark energy.<sup>6</sup> This would indicate that the empirical standardization of SN Ia brightness practiced by the SNe Ia community is not quite capable of correcting for this effect of luminosity evolution. In order to put this result on a firmer refined basis, further observations (for more host sample, for the local property at the site of SN) are definitely required. Nevertheless, until then, this work presents some serious evidence for the luminosity evolution in SN cosmology. The future direction of SN cosmology, therefore, should investigate this systematic bias before proceeding to the details of the dark energy.

<sup>6</sup> The detailed discussion on the inference of dark energy from other cosmological probes is beyond the scope of this paper. For the relevant discussion, we refer the reader to Tutusaus et al. (2017, 2019) who showed that the low- $z$  probes and combination of them are consistent with a non-accelerating universe when the SN cosmology is highly affected by luminosity evolution (as suggested in this paper). When the cosmic microwave background (i.e., high- $z$  probe) data is added in their analysis, however, a non-accelerated reconstruction is in tension with recent measurements of the Hubble constant.

## ACKNOWLEDGMENTS

We thank the anonymous referee for a number of helpful comments and suggestions. We also thank Nate Bastian, John P. Blakeslee, Aeree Chung, Pierre Demarque, Peter Garnavich, Myungkook J. Jee, Yong-Cheol Kim, Taysun Kimm, Pavel Kroupa, J. M. Diederik Kruijssen, Benjamin L’Huillier, Dongwook Lim, Martín López-Corredoira, Myeong-Gu Park, Adam G. Riess, Mickael Rigault, Arman Shafieloo, Elena Terlevich, Sukyoung K. Yi, and Suk-Jin Yoon for their comments and encouragements. We are grateful to the staff of LCO and MMT for their support during the observations. Support for this work was provided by the National Research Foundation of Korea (grants 2017R1A2B3002919, and 2017R1A5A1070354). Telescope times for this project were partially supported by K-GMT Science Program (PID: MMT\_2014\_00002, GS-2015B-Q-41, GN-2016A-Q-51) of Korea Astronomy and Space Science Institute. Y.K acknowledges support from the YONSEI University Graduate School Research Scholarship 2017. Y.-L.K. acknowledges support from the European Research Council (ERC) under the European Union’s Horizon 2020 research and innovation programme (grant agreement No. 759194 - USNAC). This research has made use of the NASA/IPAC Extragalactic Database (NED) which is operated by the Jet Propulsion Laboratory, California Institute of Technology, under contract with the National Aeronautics and Space Administration. We acknowledge the usage of the HyperLeda (<http://leda.univ-lyon1.fr>), SDSS (<http://www.sdss.org>), GALEX (<http://galex.stsci.edu>), DESI Legacy Imaging Surveys (<http://legacysurvey.org>), and unWISE (<http://unwise.me>) databases.

## REFERENCES

- Abolfathi, B., Aguado, D. S., Aguilar, G., et al. 2018, *ApJS*, 235, 42
- Aniano, G., Draine, B. T., Gordon, K. D., et al. 2011, *PASP*, 123, 1218
- Behroozi, P. S., Wechsler, R. H., & Conroy, C. 2013, *ApJ*, 770, 57
- Bernard, E. J. 2018, *Rediscovering Our Galaxy*, 158
- Betoule, M., Kessler, R., Guy, J., et al. 2014, *A&A*, 568, A22
- Burns, C. R., Stritzinger, M., Phillips, M. M., et al. 2014, *ApJ*, 789, 32
- Cappellari, M., & Emsellem, E. 2004, *PASP*, 116, 138
- Cappellari, M., Emsellem, E., Krajnović, D., et al. 2011, *MNRAS*, 413, 813
- Cardiel, N., Gorgas, J., Cenarro, J., et al. 1998, *A&AS*, 127, 597
- Childress, M., Aldering, G., Antilogus, P., et al. 2013, *ApJ*, 770, 108
- Childress, M. J., Wolf, C., & Zahid, H. J. 2014, *MNRAS*, 445, 1898
- Chung, C., Yoon, S.-J., Lee, S.-Y., et al. 2013, *ApJS*, 204, 3
- Chung, C., Yoon, S.-J., & Lee, Y.-W. 2017, *ApJ*, 842, 91
- Cid Fernandes, R., Mateus, A., Sodré, L., et al. 2005, *MNRAS*, 358, 363
- D’Andrea, C. B., Gupta, R. R., Sako, M., et al. 2011, *ApJ*, 743, 172
- Denicoló, G., Terlevich, R., Terlevich, E., et al. 2005, *MNRAS*, 356, 1440
- Dey, A., Schlegel, D. J., Lang, D., et al. 2019, *AJ*, 157, 168
- Drell, P. S., Loredó, T. J., & Wasserman, I. 2000, *ApJ*, 530, 593
- Faber, S. M., Worthey, G., & Gonzales, J. J. 1992, *The Stellar Populations of Galaxies*, 255
- Ferramacho, L. D., Blanchard, A., & Zolnierowski, Y. 2009, *A&A*, 499, 21
- Galbany, L., Stanishev, V., Mourão, A. M., et al. 2014, *A&A*, 572, A38
- Gallagher, J. S., Garnavich, P. M., Caldwell, N., et al. 2008, *ApJ*, 685, 752
- Graves, G. J., Faber, S. M., & Schiavon, R. P. 2009, *ApJ*, 698, 1590
- Graves, G. J., & Schiavon, R. P. 2008, *ApJS*, 177, 446
- Greggio, L. 1997, *MNRAS*, 285, 151
- Guy, J., Astier, P., Baumont, S., et al. 2007, *A&A*, 466, 11
- Guérou, A., Emsellem, E., Krajnović, D., et al. 2016, *A&A*, 591, A143
- Gupta, R. R., D’Andrea, C. B., Sako, M., et al. 2011, *ApJ*, 740, 92
- Hamuy, M., Trager, S. C., Pinto, P. A., et al. 2000, *AJ*, 120, 1479
- Hicken, M., Wood-Vasey, W. M., Blondin, S., et al. 2009, *ApJ*, 700, 1097
- Howell, D. A. 2001, *ApJL*, 554, L193

- Howell, D. A., Sullivan, M., Brown, E. F., et al. 2009, *ApJ*, 691, 661
- Jha, S., Riess, A. G., & Kirshner, R. P. 2007, *ApJ*, 659, 122
- Johansson, J., Thomas, D., Pforr, J., et al. 2013, *MNRAS*, 435, 1680
- Jones, D. O., Riess, A. G., & Scolnic, D. M. 2015, *ApJ*, 812, 31
- Joo, S.-J., & Lee, Y.-W. 2013, *ApJ*, 762, 36
- Kang, Y., Kim, Y.-L., Lim, D., et al. 2016, *ApJS*, 223, 7 (Paper I)
- Kelly, B. C. 2007, *ApJ*, 665, 1489
- Kelly, P. L., Hicken, M., Burke, D. L., et al. 2010, *ApJ*, 715, 743
- Kessler, R., Bernstein, J. P., Cinabro, D., et al. 2009, *PASP*, 121, 1028
- Kim, S., Yoon, S.-J., Chung, C., et al. 2013, *ApJ*, 768, 138
- Kim, Y.-L., Kang, Y., & Lee, Y.-W. 2019, arXiv e-prints, arXiv:1908.10375
- Kim, Y.-L., Smith, M., Sullivan, M., et al. 2018, *ApJ*, 854, 24
- Kuntschner, H., Emsellem, E., Bacon, R., et al. 2010, *MNRAS*, 408, 97
- Kuntschner, H., Lucey, J. R., Smith, R. J., et al. 2001, *MNRAS*, 323, 615
- Lang, D. 2014, *AJ*, 147, 108
- Lee, Y.-W., Joo, S.-J., Han, S.-I., et al. 2005, *ApJL*, 621, L57
- Linden, S., Virey, J.-M., & Tilquin, A. 2009, *A&A*, 506, 1095
- Makarov, D., Prugniel, P., Terekhova, N., et al. 2014, *A&A*, 570, A13
- Martin, D. C., Fanson, J., Schiminovich, D., et al. 2005, *ApJL*, 619, L1
- Neill, J. D., Sullivan, M., Howell, D. A., et al. 2009, *ApJ*, 707, 1449
- Neistein, E., van den Bosch, F. C., & Dekel, A. 2006, *MNRAS*, 372, 933
- Nolan, L. A., Dunlop, J. S., Panter, B., et al. 2007, *MNRAS*, 375, 371
- Pan, Y.-C., Sullivan, M., Maguire, K., et al. 2014, *MNRAS*, 438, 1391
- Perlmutter, S., Aldering, G., Goldhaber, G., et al. 1999, *ApJ*, 517, 565
- Perlmutter, S., Gabi, S., Goldhaber, G., et al. 1997, *ApJ*, 483, 565
- Phillips, M. M. 1993, *ApJL*, 413, L105
- Riess, A. G., Filippenko, A. V., Challis, P., et al. 1998, *AJ*, 116, 1009
- Riess, A. G., Kirshner, R. P., Schmidt, B. P., et al. 1999, *AJ*, 117, 707
- Riess, A. G., Press, W. H., & Kirshner, R. P. 1996, *ApJ*, 473, 88
- Riess, A. G., Strolger, L.-G., Tonry, J., et al. 2004, *ApJ*, 607, 665
- Rigault, M., Aldering, G., Kowalski, M., et al. 2015, *ApJ*, 802, 20
- Rigault, M., Brinnel, V., Aldering, G., et al. 2018, arXiv e-prints, arXiv:1806.03849
- Rigault, M., Copin, Y., Aldering, G., et al. 2013, *A&A*, 560, A66

- Roman, M., Hardin, D., Betoule, M., et al. 2018, *A&A*, 615, A68
- Rose, B. M., Garnavich, P. M., & Berg, M. A. 2019, *ApJ*, 874, 32
- Sánchez-Blázquez, P., Gorgas, J., Cardiel, N., et al. 2006, *A&A*, 457, 787
- Sarzi, M., Falcón-Barroso, J., Davies, R. L., et al. 2006, *MNRAS*, 366, 1151
- Scalzo, R. A., Parent, E., Burns, C., et al. 2019, *MNRAS*, 483, 628
- Schiavon, R. P. 2007, *ApJS*, 171, 146
- Schmidt, B. P., Suntzeff, N. B., Phillips, M. M., et al. 1998, *ApJ*, 507, 46
- Scolnic, D., & Kessler, R. 2016, *ApJL*, 822, L35
- Scott, N., Brough, S., Croom, S. M., et al. 2017, *MNRAS*, 472, 2833
- Serra, P., & Trager, S. C. 2007, *MNRAS*, 374, 769
- Shapiro, K. L., Falcón-Barroso, J., van de Ven, G., et al. 2010, *MNRAS*, 402, 2140
- Spavone, M., Iodice, E., Capaccioli, M., et al. 2018, *ApJ*, 864, 149
- Sullivan, M., Conley, A., Howell, D. A., et al. 2010, *MNRAS*, 406, 782
- Sullivan, M., Guy, J., Conley, A., et al. 2011, *ApJ*, 737, 102
- Sullivan, M., Le Borgne, D., Pritchet, C. J., et al. 2006, *ApJ*, 648, 868
- Suzuki, N., Rubin, D., Lidman, C., et al. 2012, *ApJ*, 746, 85
- Thomas, D., Maraston, C., Bender, R., et al. 2005, *ApJ*, 621, 673
- Thomas, D., Maraston, C., & Johansson, J. 2011, *MNRAS*, 412, 2183
- Thomas, D., Maraston, C., Schawinski, K., et al. 2010, *MNRAS*, 404, 1775
- Tinsley, B. M. 1968, *ApJ*, 151, 547
- Trager, S. C., Faber, S. M., Worthey, G., et al. 2000, *AJ*, 119, 1645
- Trager, S. C., Worthey, G., Faber, S. M., et al. 1998, *ApJS*, 116, 1
- Tutusaus, I., Lamine, B., & Blanchard, A. 2019, *A&A*, 625, A15
- Tutusaus, I., Lamine, B., Dupays, A., et al. 2017, *A&A*, 602, A73
- Umeda, H., Nomoto, K., Kobayashi, C., et al. 1999, *ApJL*, 522, L43
- Worthey, G. 1994, *ApJS*, 95, 107
- Worthey, G., Faber, S. M., Gonzalez, J. J., et al. 1994, *ApJS*, 94, 687
- Worthey, G., & Ottaviani, D. L. 1997, *ApJS*, 111, 377
- Yi, S. K., Yoon, S.-J., Kaviraj, S., et al. 2005, *ApJL*, 619, L111
- Zibetti, S., Gallazzi, A. R., Hirschmann, M., et al. 2019, arXiv e-prints, arXiv:1906.02209

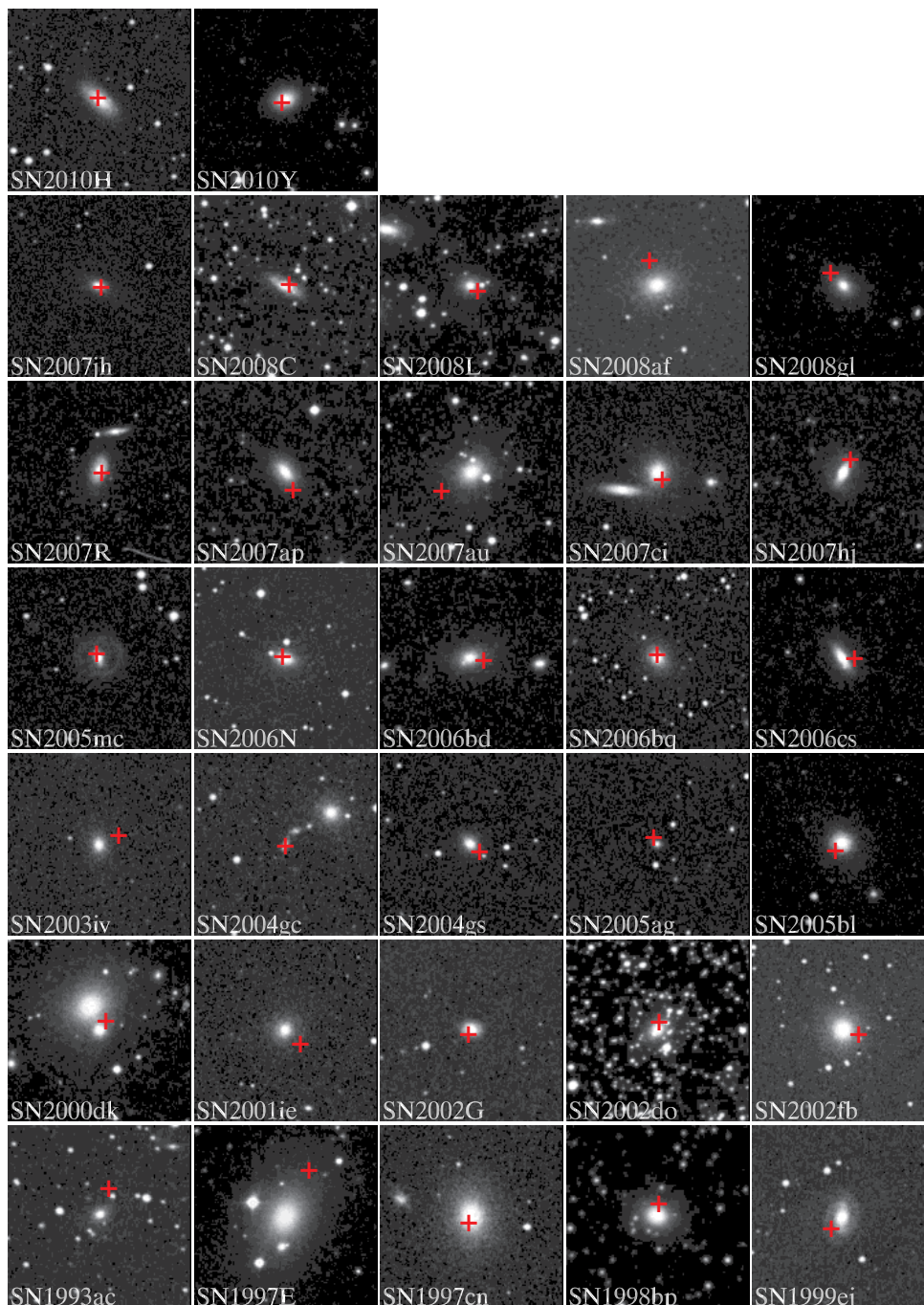


**Figure 1.** The DSS images of our host galaxy sample observed at MMT 6.5-m. Each of host galaxies is placed at the center of an image, and the name and the position (the red cross) of SN Ia are given in each panel. The images of host galaxies observed at LCO can be found in Figure 1 of Paper I.

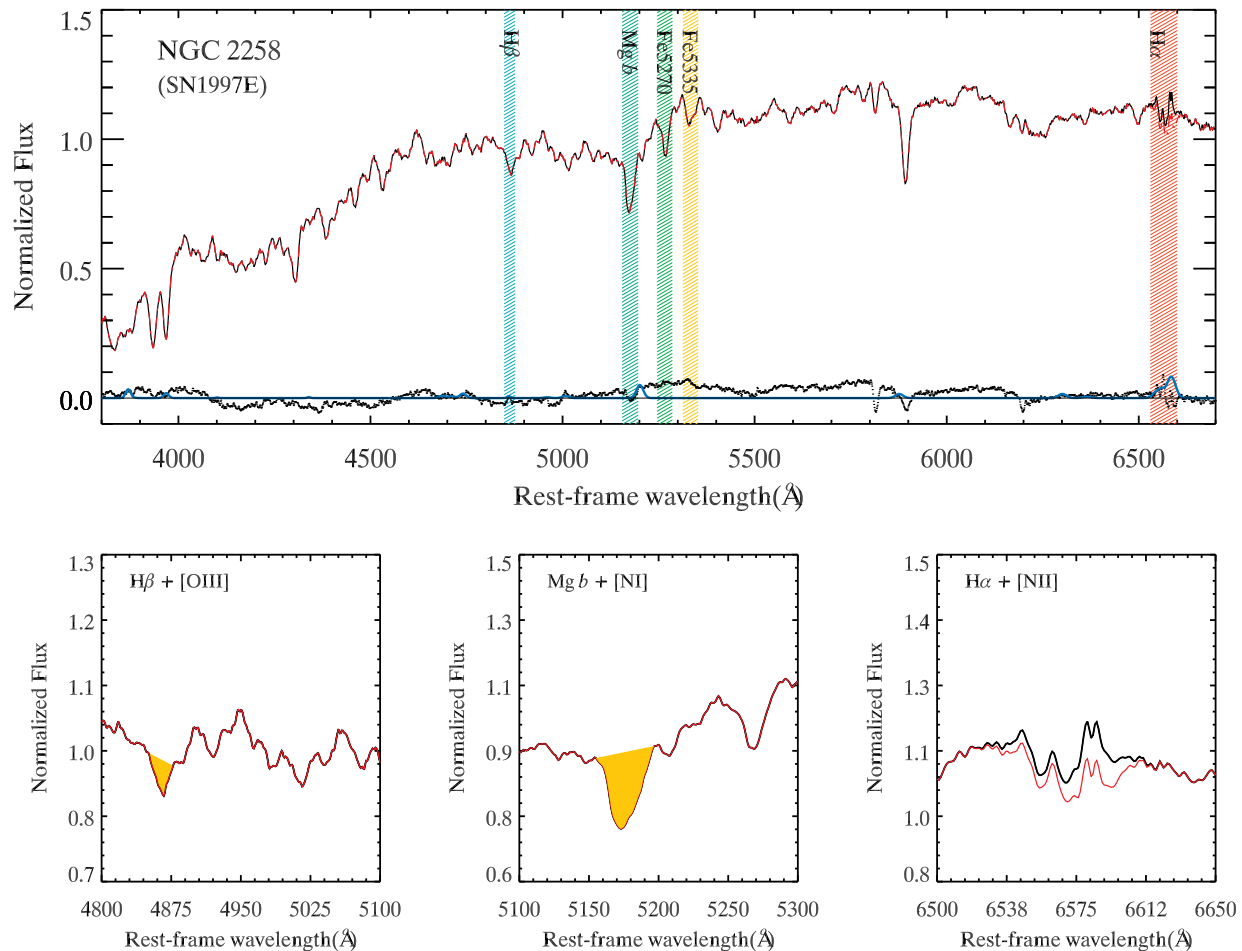


**Figure 2.** Example of our host galaxy spectra for NGC 2258, a host of SN 1997E. The black and red solid lines are fully-calibrated spectra in the rest-frame, before and after the emission correction, respectively. The upper panel shows the entire wavelength coverage of our observation, where the absorption bands for  $H\beta$ ,  $Mg\ b$ ,  $Fe5270$ ,  $Fe5335$ , and  $H\alpha$  are indicated in color shades. The gray line at the bottom of the panel shows the difference between the best-fit model and our spectrum, where the detected emission lines (cyan) are overlapped on the residuals. The lower panels show the spectral regions around  $H\beta + [O\ III]$  (4900-5100 Å),  $Mg\ b + [N\ I]$  (5100-5300 Å), and  $H\alpha + [N\ II]$  (6500-6650 Å), where the orange shades indicate the areas for the line strength measurements

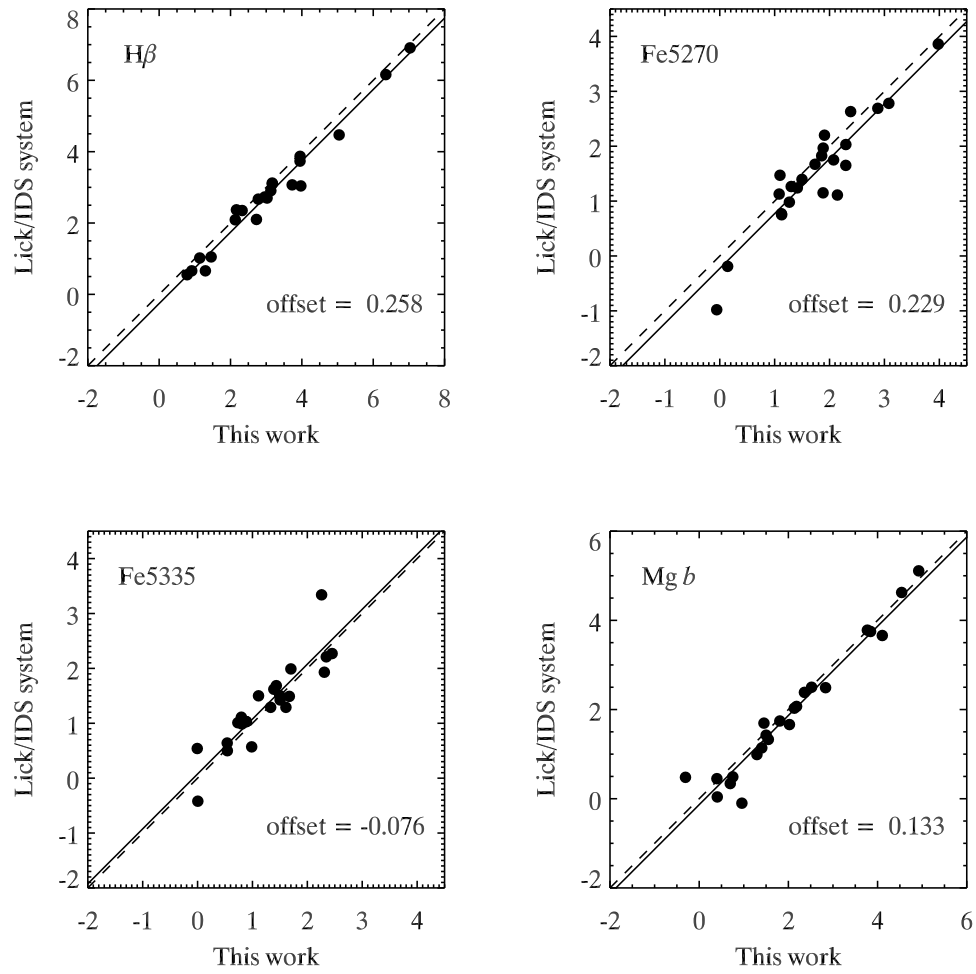


**Figure 3.** Comparison of Lick indices measured in this study for the Lick/IDS standard stars with those in [Worthey et al. \(1994\)](#) and [Worthey & Ottaviani \(1997\)](#). The dashed line is for the one-to-one relation, while the solid line shows the mean offset (our work-Lick/IDS system) which is given in each panel.



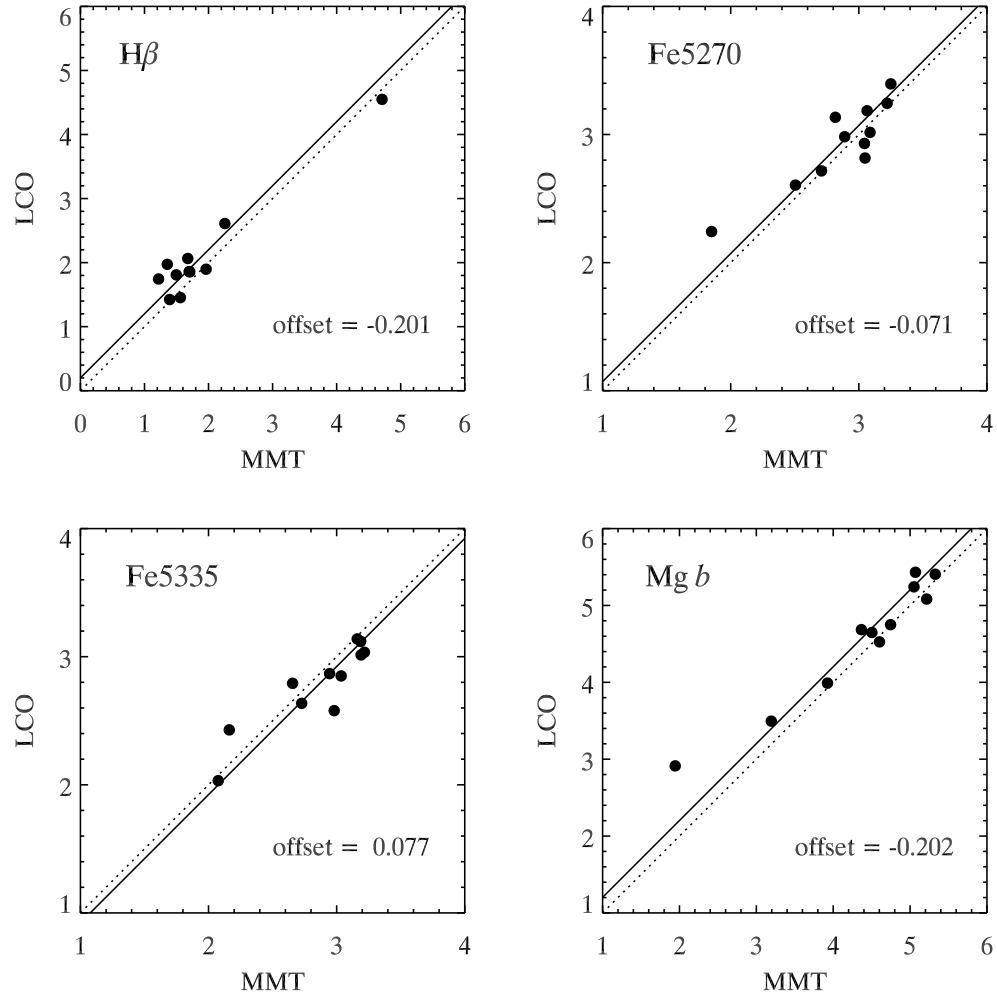


**Figure 4.** Same as Figure 3, but for the common galaxies observed both at MMT (x-axis) and LCO (y-axis). The mean offset (MMT-LCO observations) is given in each panel.

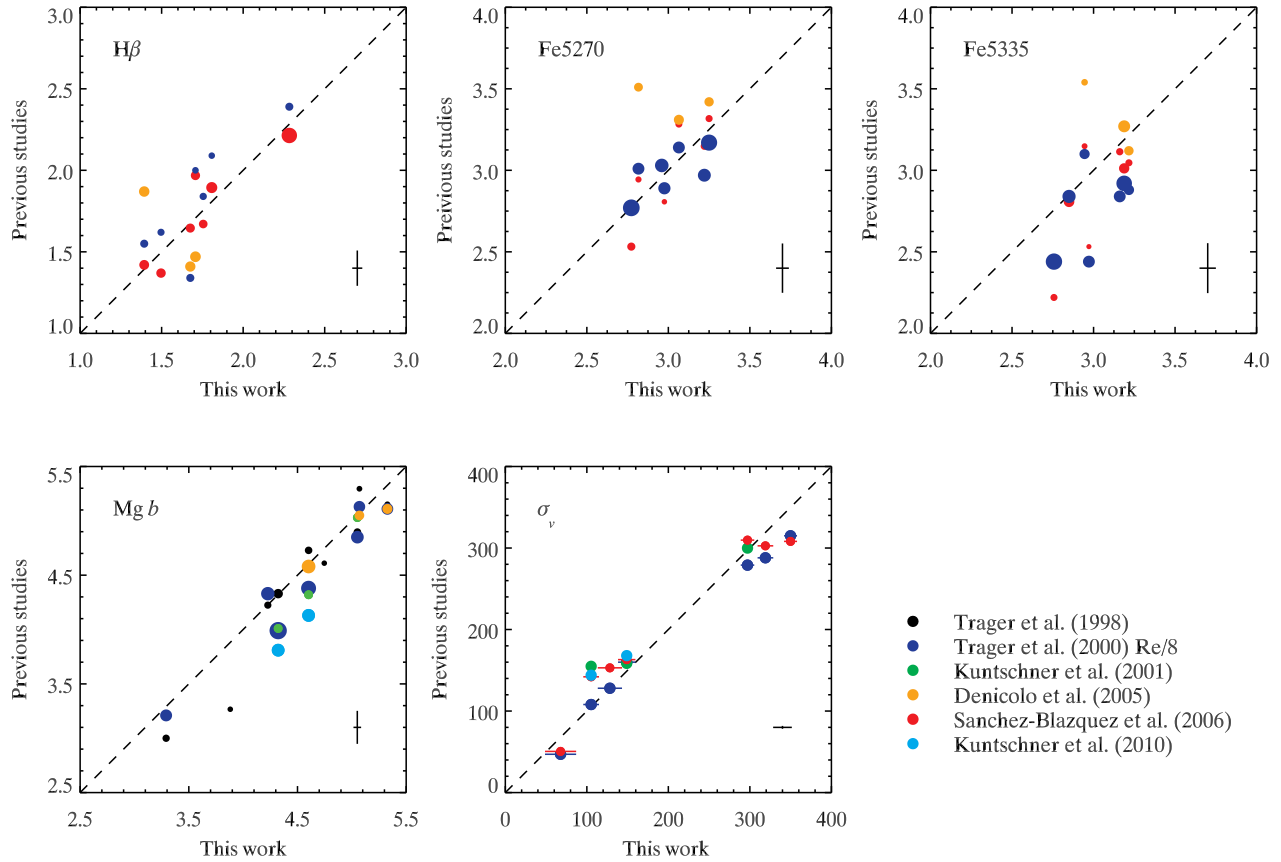


**Figure 5.** Comparison of Lick indices ( $H\beta$ , Fe5270, Fe5335, and Mg b in  $\text{\AA}$ ) and velocity dispersion ( $\sigma_v$  in  $\text{km s}^{-1}$ ) measured in this study for the non-host early-type galaxies observed at MMT 6.5-m with those from the literature. The dashed lines represent the one-to-one relations. The size of the symbol is inversely proportional to the error, and the typical errors for each value are indicated in the lower right corner of each panel.

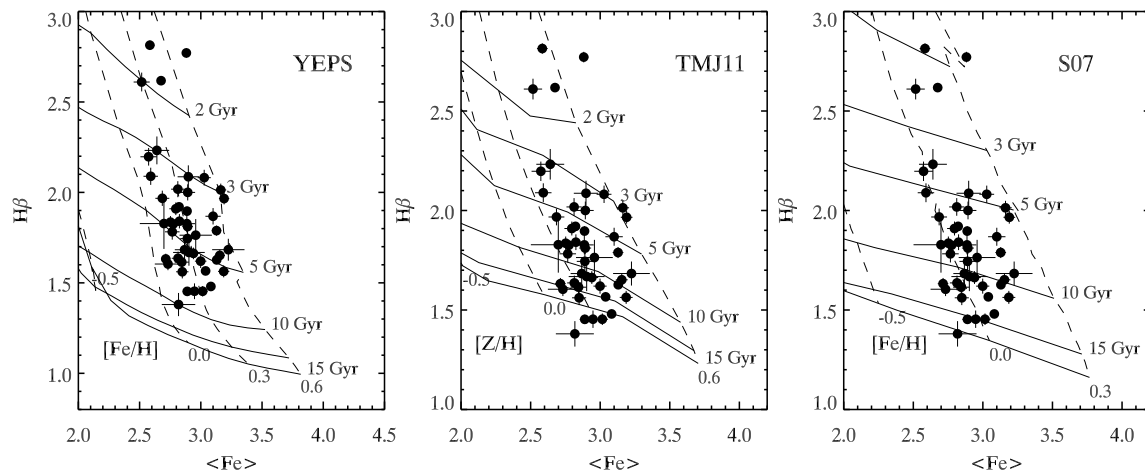


**Figure 6.** Determination of luminosity-weighted mean age and metallicity for our sample of early-type host galaxies. Filled circles represent measured indices for our host galaxy sample which are overlaid with their errors on the model grids ( $[\alpha/\text{Fe}] = 0.3$ ) from three different sets of EPS models (YEPS, TMJ11, and S07). The solid horizontal lines are for common ages, while the dashed vertical lines are for the same metallicity ( $[\text{Fe}/\text{H}]$  for YEPS and S07,  $[\text{Z}/\text{H}]$  for TMJ11).

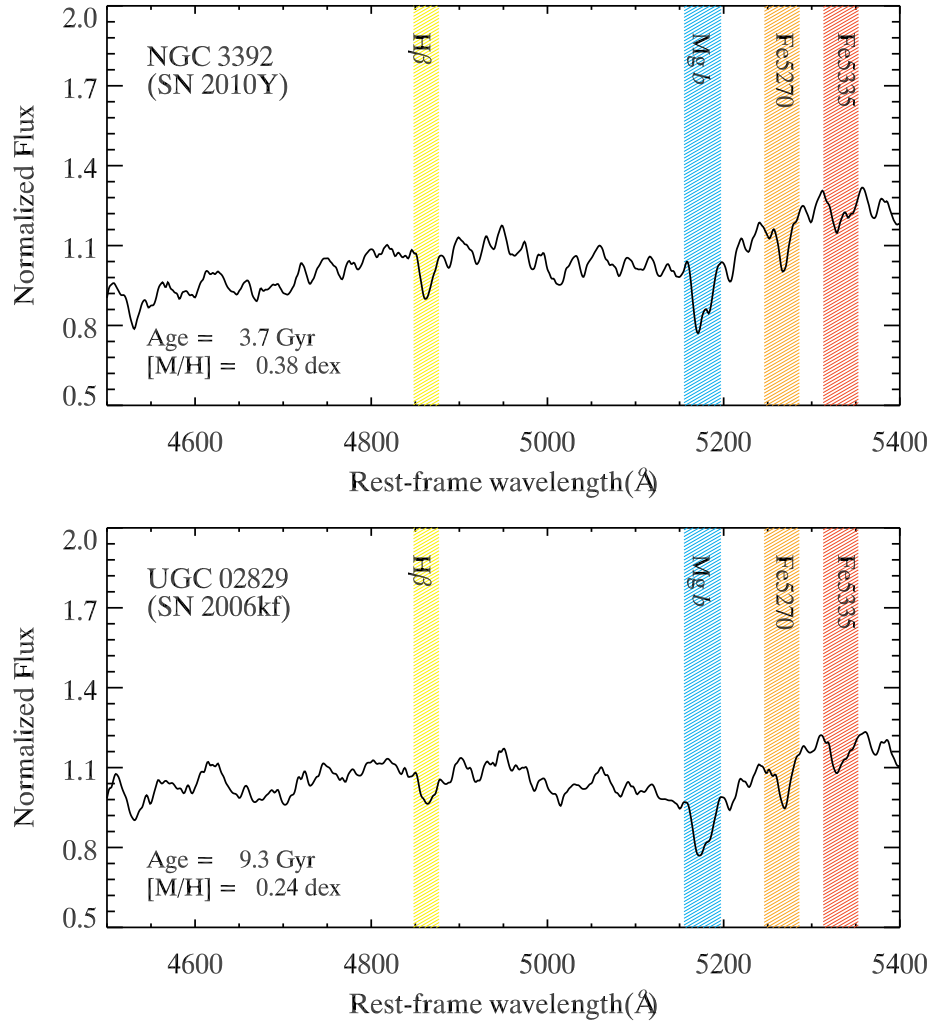


**Figure 7.** Example of typical spectra for the relatively young (NGC 3392; upper) and old host galaxies (UGC 02829; lower). Note the difference in the depth of H $\beta$  index. Population age and metallicity are given in each panel. Colored shades are absorption bands for H $\beta$ , Mg *b*, Fe5270, and Fe5335, respectively.

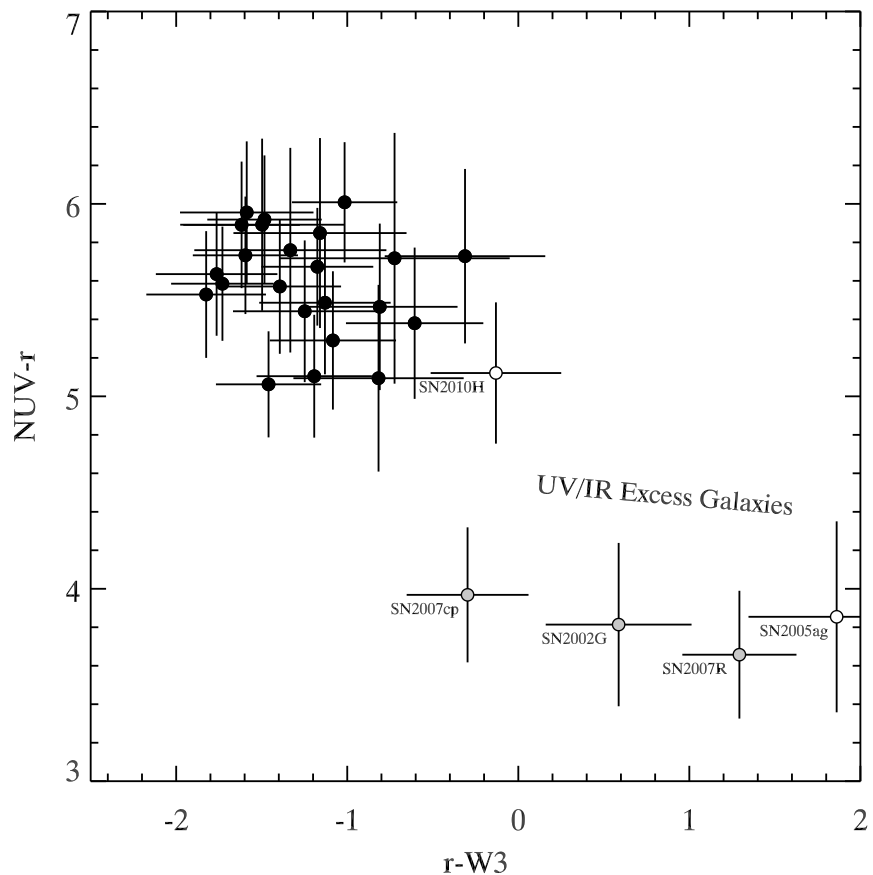


**Figure 8.** UV-optical-IR color-color diagram of the host galaxies used to select out non-genuine early-type galaxies showing features of the recent episode of starburst. The grey circles are for galaxies showing excess emissions both in  $NUV$  and  $W3$ , and the white circles denote the rejuvenated galaxies (age  $< 2.5$  Gyr). Mean isophotal colors at the effective radii are measured from the PSF-matched (Aniano et al. 2011) multi-wavelength image.

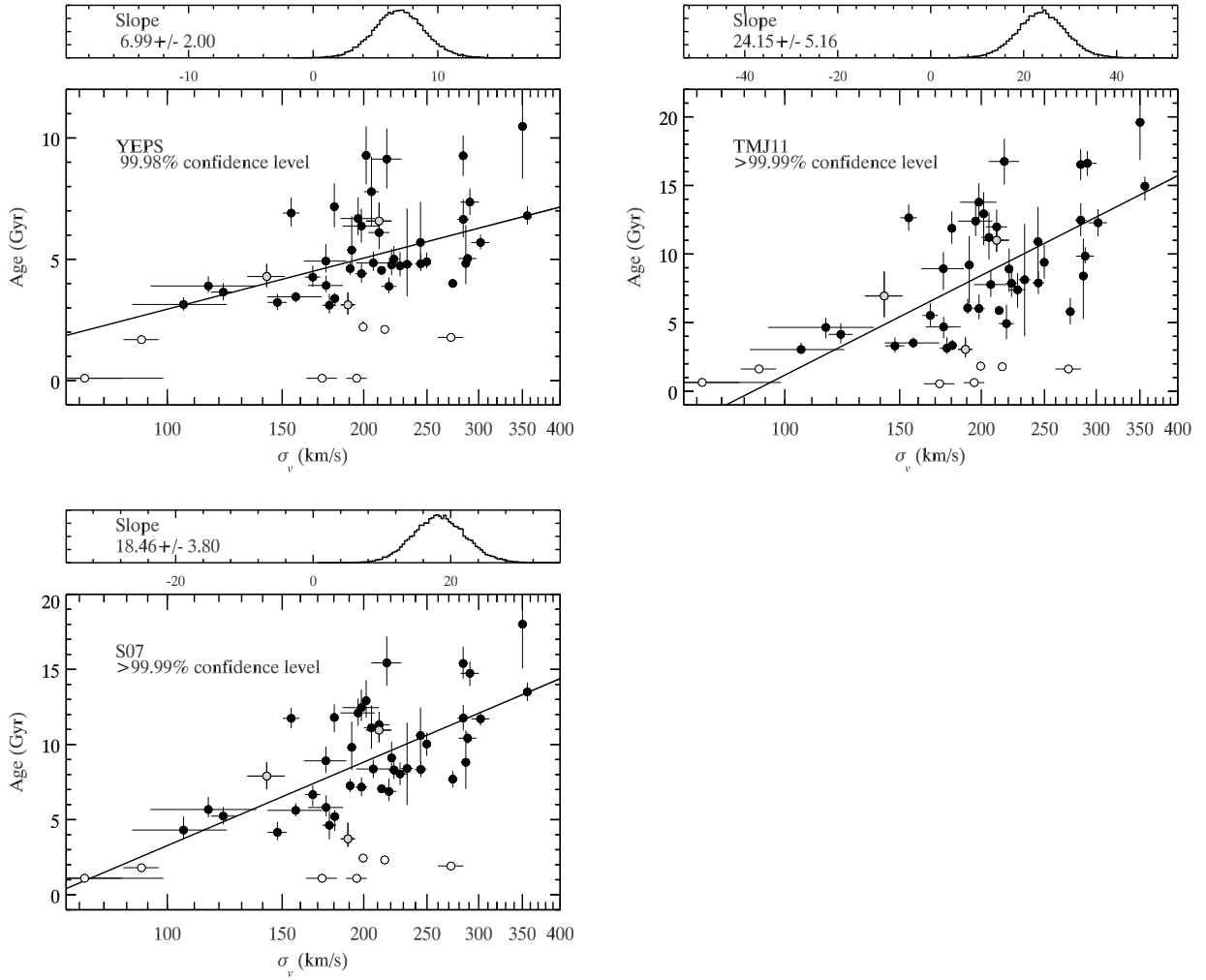


**Figure 9.** Correlation between velocity dispersion ( $\sigma_v$ ) and stellar population age for our sample of host galaxies. Population ages of galaxies were determined using YEPS, TMJ11, and S07 models, respectively. The black solid line is the regression line obtained from the posterior median estimate of MCMC analyses, and the confidence level of the correlation is given in each panel. Non-genuine early-type galaxies excluded from our final analyses are denoted by the white and grey circles for the rejuvenated and UV/IR excess galaxies, respectively.

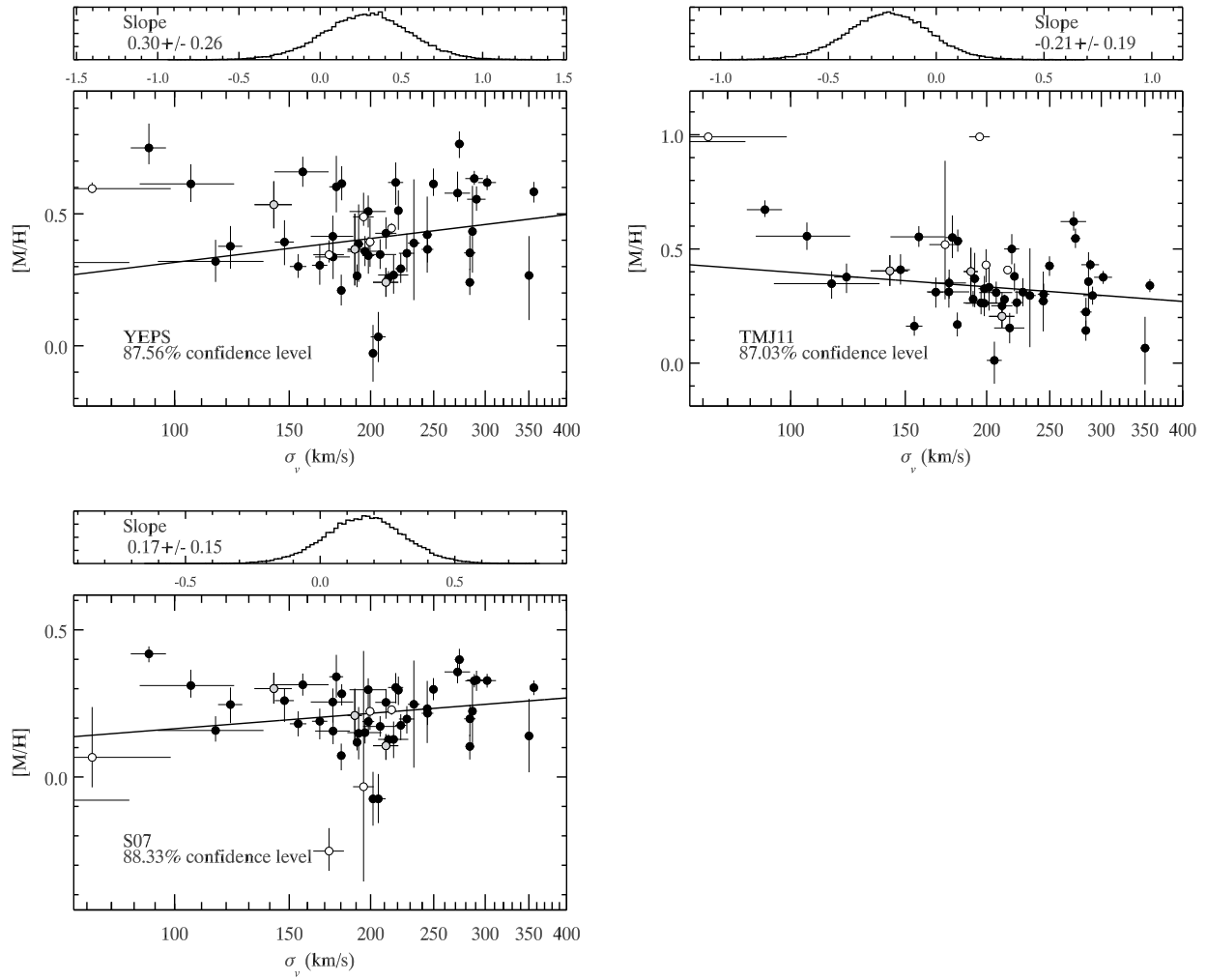


**Figure 10.** Same as Figure 9, but for the metallicity  $[M/H]$  which shows no significant correlation.

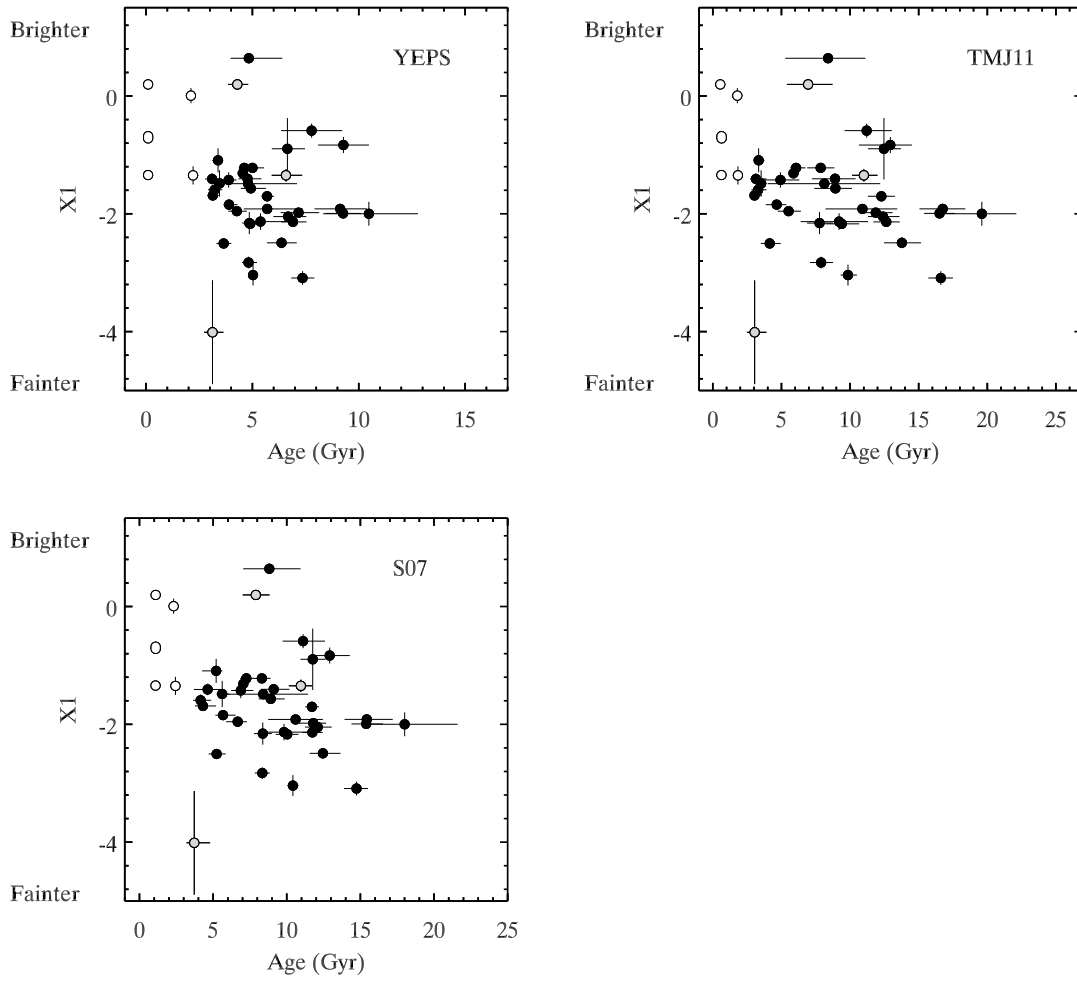


**Figure 11.** Correlation of population age for host galaxies with SN stretch factor ( $X_1$ ). Population ages from YEPS, TMJ11, and S07 models are shown on each panel, respectively. Non-genuine early-type galaxies excluded from our final analyses are denoted by the white and grey circles for rejuvenated galaxies and UV/IR excess galaxies, respectively.



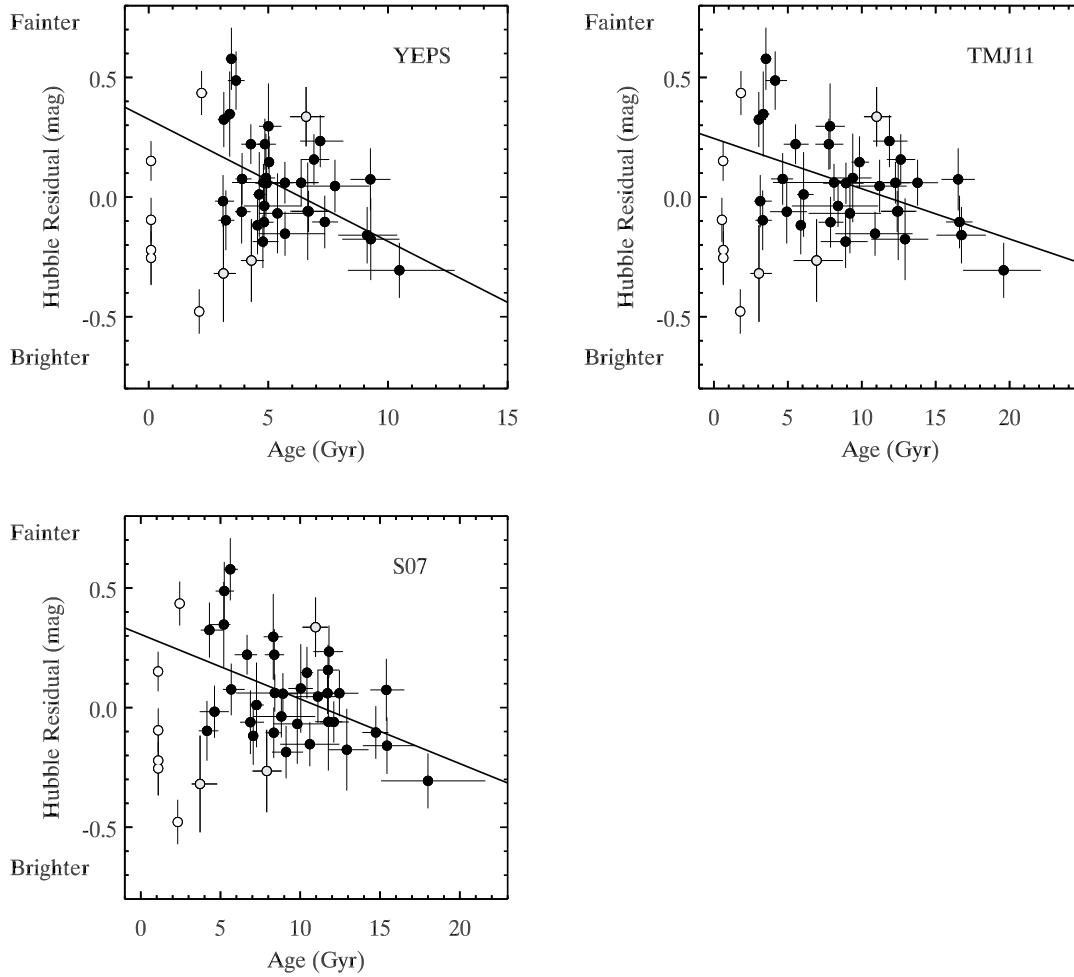


**Figure 12.** Correlation between population age of host galaxy and Hubble residual of SN Ia. Population ages from YEPS, TMJ11, and S07 models are shown on each panel, respectively. Non-genuine early-type galaxies excluded from our final analyses are denoted by the white and grey circles for rejuvenated galaxies and UV/IR excess galaxies, respectively. The solid line is the regression fit obtained from MCMC analysis only for our final sample.

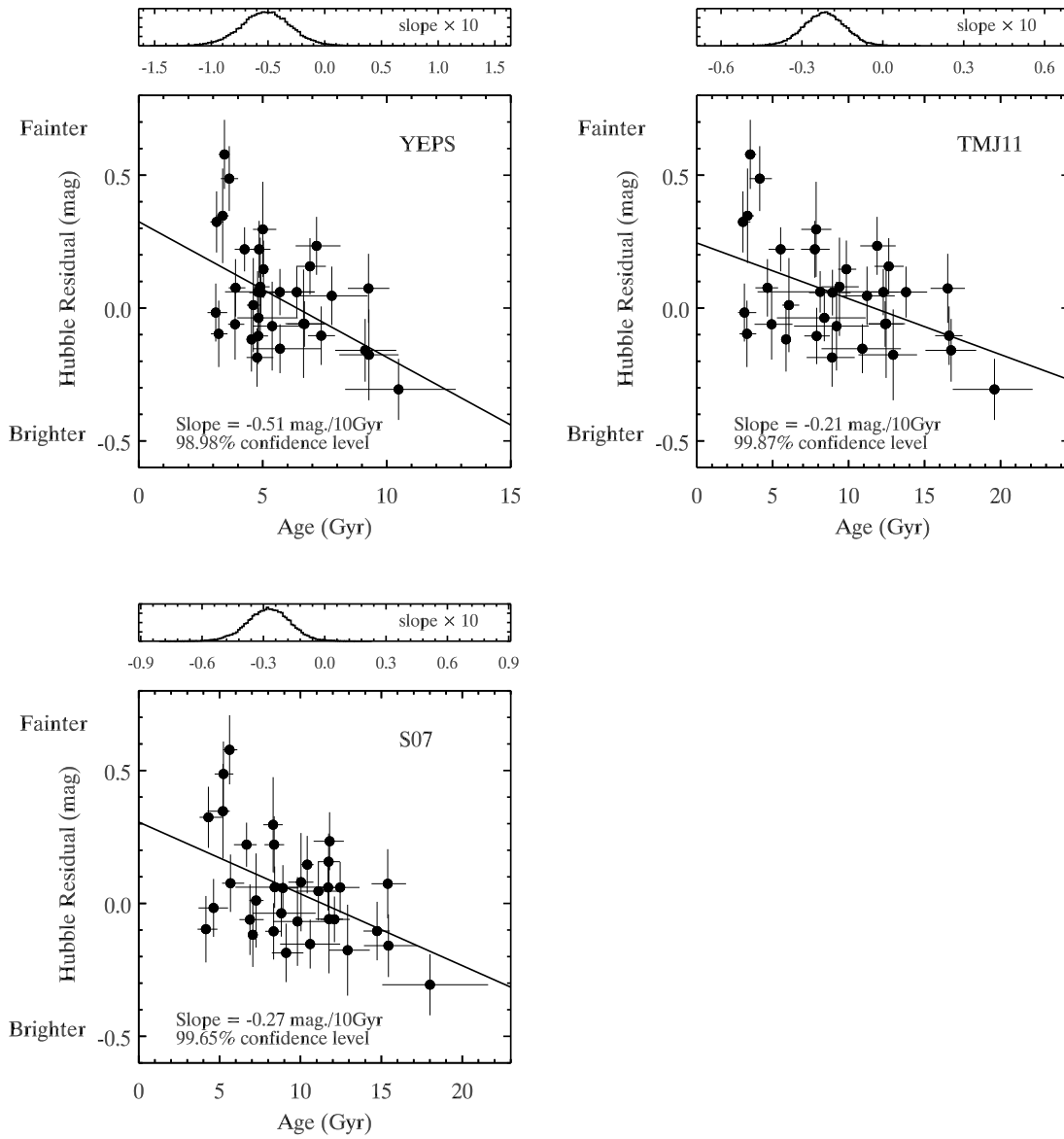


**Figure 13.** Same as Figure 12, but only for our final sample. The difference in Hubble residual per 10 Gyr and the confidence level are given in each panel together with the posterior slope distribution.

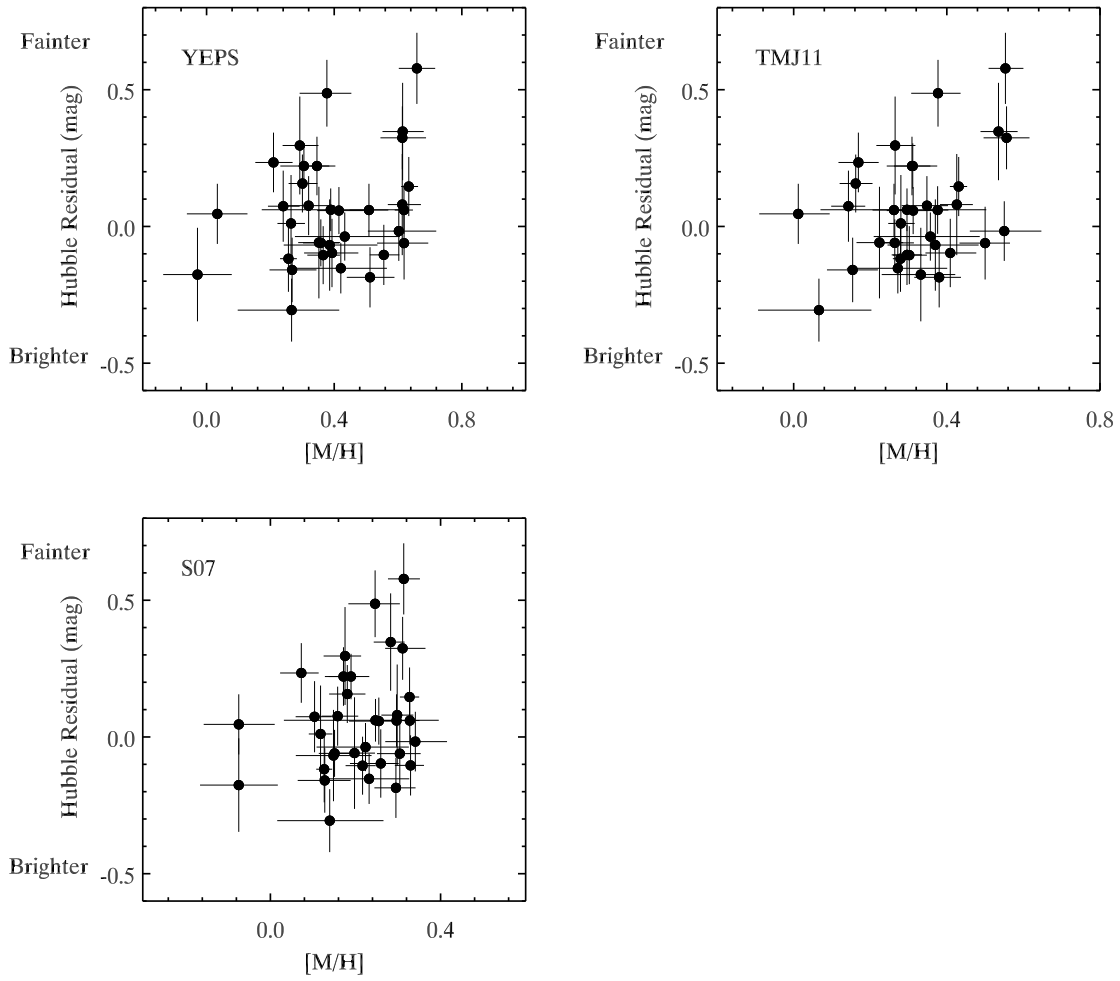


**Figure 14.** Same as Figure 13, but for the metallicity  $[M/H]$  which shows no significant correlation.

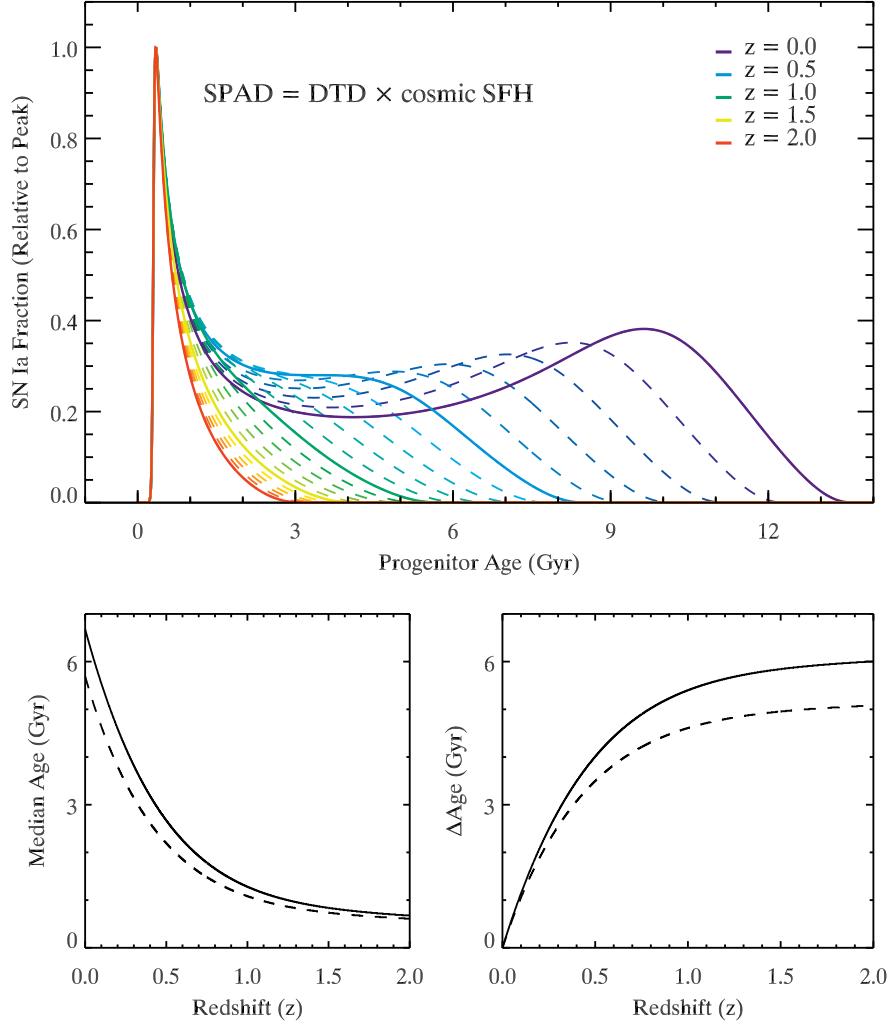


**Figure 15.** SN Ia progenitor age distribution (SPAD) as a function of redshift calculated following Childress et al. (2014). This is for the sample of SNe Ia arising at a given epoch of cosmic time summed over all galaxy types. The upper panel shows the distributions in steps of  $\Delta z = 0.1$ . The lower panels are the median value of the age distribution (left) and the difference with respect to  $z = 0$  (right). To calculate a look-back time at a given redshift, we implicitly adopted the  $\Lambda$ CDM cosmological model ( $\Omega_M = 0.27$ ,  $\Omega_\Lambda = 0.73$ ), while the dashed lines in the lower panels show the results for the cosmological model without  $\Lambda$  ( $\Omega_M = 0.27$ ,  $\Omega_\Lambda = 0.00$ ).

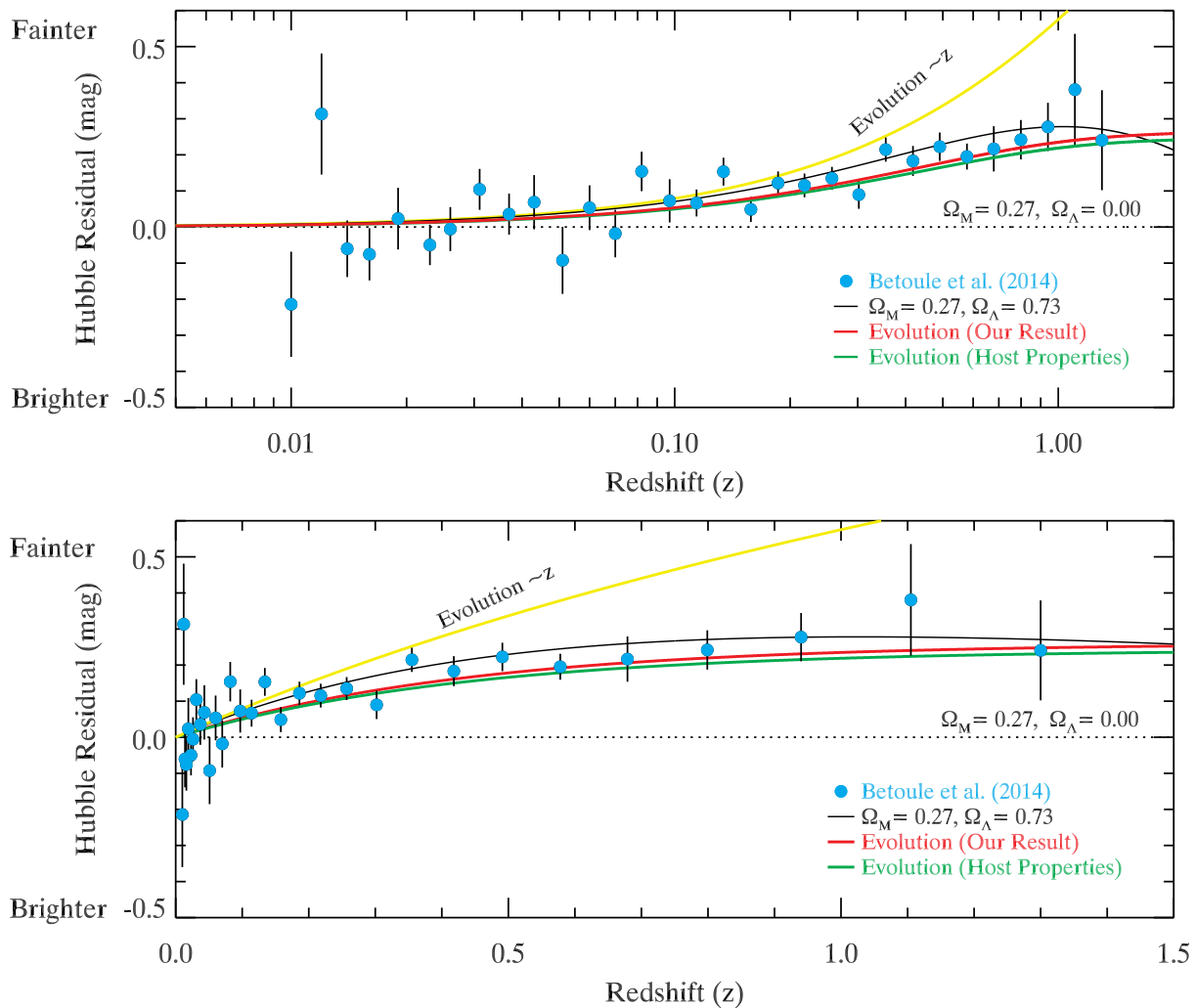


**Figure 16.** The luminosity evolution in SN cosmology predicted by our age dating of early-type host galaxies. The Hubble residuals are calculated with respect to the cosmological model without  $\Lambda$  ( $\Omega_M = 0.27$ ,  $\Omega_\Lambda = 0.00$ ; the black dotted line). Assuming this model, the red line is the evolution curve based only on the age dating of early-type host galaxies, while the green line is produced using the mean value of  $\Delta\text{HR}/\Delta\text{age}$  from the four different studies on host properties. Note that our evolution curve is substantially different from that simply proportional to redshift (yellow line). The cyan circles are the binned SN data from [Betoule et al. \(2014\)](#). The comparison of our evolution curves with SN data shows that the luminosity evolution can mimic a significant fraction of the Hubble residual used in the discovery and inference of the dark energy (see the black solid line).

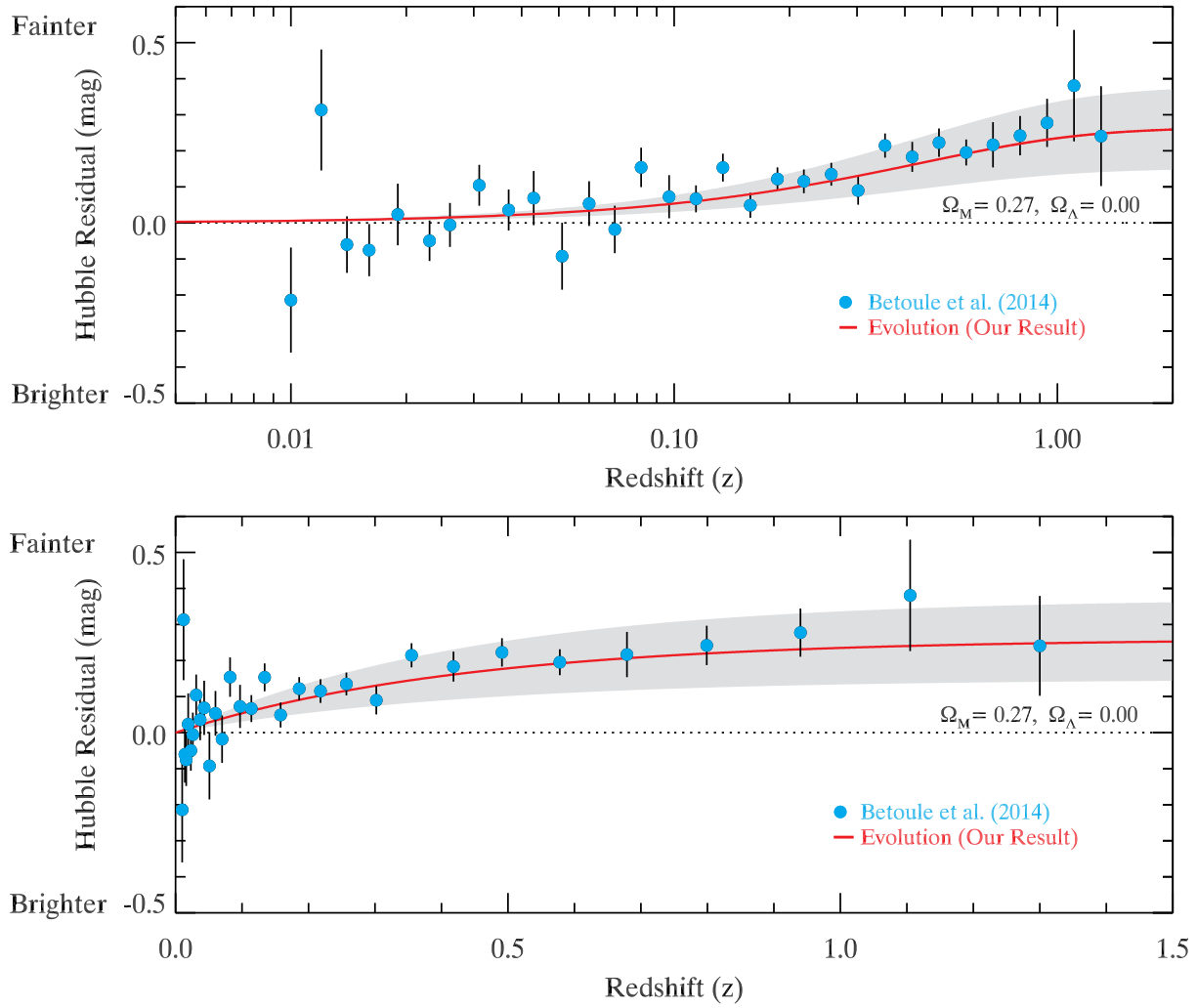


**Figure 17.** Same as Figure 16, but  $1\sigma$  significance interval is added to our evolution curve (the grey shade).

**Table 1.** Our Sample of Early-type Host Galaxies<sup>a</sup>

SN	Galaxy	R.A.	Decl.	$B^T$	Morphology	$z$	PA	Exposure	Telescope
		(J2000)	(J2000)	(mag)			( $^\circ$ )	( $N \times s$ )	
SN 1990af	2MASX J21345926-6244143	21:34:59.31	-62:44:14.5	16.07	SB0	0.050575	50	$6 \times 3600$	LCO
SN 1992bo	ESO 352-G057	01:22:02.41	-34:11:48.4	14.76	SB(s)0 <sup>+</sup> 0 <sup>+</sup> pec	0.018983	12	$3 \times 3600$	LCO
SN 1993ac	CGCG 307-023	05:46:24.64	+63:21:32.6	16.16	E	0.049000	135	$3 \times 900$	MMT
SN 1993ag	2MASX J10033546-3527410	10:03:35.46	-35:27:41.0	16.86	E3/S01	0.049094	80	$11 \times 3600$	LCO
SN1994M	NGC 4493	12:31:08.37	+00:36:49.3	14.78	SA?0-pec	0.023159	0	$6 \times 3600 + 2 \times 600 + 2 \times 900$	LCO, MMT
SN 1997E	NGC 2258	06:47:45.80	+74:28:54.0	13.01	SA(r)0 <sup>+</sup> 0 <sup>+</sup>	0.013539	155	$3 \times 900$	MMT
SN 1997cn	NGC 5490	14:09:57.29	+17:32:44.0	13.06	E	0.016195	5	$2 \times 600 + 3 \times 900$	MMT
SN 1998bp	NGC 6495	17:54:50.76	+18:19:36.9	13.85	E	0.010431	75	$3 \times 600$	MMT
SN 1999ej	NGC 0495	01:22:56.00	+33:28:18.0	13.68	(R')SB(s)0/a	0.013723	140	$3 \times 900$	MMT
SN 2000dk	NGC 0382	01:07:23.87	+32:24:13.9	14.48	E:HII	0.017442	135	$3 \times 900$	MMT
SN 2001ie	UGC 05542	10:16:53.06	+60:17:05.6	14.83	E:	0.030738	195	$2 \times 600$	MMT
SN 2002G	CGCG 189-024	13:07:54.81	+34:05:13.6	15.22	E	0.033737	75	$2 \times 600$	MMT
SN 2002dj	NGC 5018	13:13:01.03	-19:31:05.5	11.69	E3:	0.009393	100	$3 \times 1800 + 4 \times 3600$	LCO
SN 2002do	MCG +07-41-001	19:56:12.86	+40:26:02.3	14.69	E1:	0.015881	140	$2 \times 600$	MMT
SN 2002fb	NGC 0759	01:57:50.33	+36:20:35.2	13.83	E	0.015567	70	$3 \times 900$	MMT
SN 2003ch	UGC 03787	07:17:57.56	+09:41:21.6	15.56	E-S0	0.028620	0	$3 \times 1800 + 1 \times 3600, 2 \times 900$	LCO, MMT
SN 2003ic	MCG -02-02-086	00:41:50.47	-09:18:11.3	14.6	cD;BrClG	0.055672	130	$6 \times 3600$	LCO
SN 2003iv	UGC 02320 NOTES01	02:50:08.84	+12:50:37.0	15.79	E <sup>b</sup>	0.034307	110	$3 \times 900$	MMT
SN 2004gc	ARP327NED04	05:21:49.79	+06:40:37.3	18.44	SA0-:	0.032089	160	$2 \times 1200$	MMT
SN 2004gs	MCG +03-22-020	08:38:23.85	+17:37:52.8	15.21	S0?	0.027425	150	$3 \times 900$	MMT
SN 2005ag	2MASX J14564322+0919361	14:56:43.21	+09:19:36.4	16.62	SBbc <sup>c</sup>	0.079665	85	$1 \times 1800$	MMT

Table 1 continued on next page

Table 1 (*continued*)

SN	Galaxy	R.A. (J2000)	Decl. (J2000)	$B^T$ (mag)	Morphology	$z$	PA ( $^\circ$ )	Exposure ( $N \times s$ )	Telescope
SN 2005al	NGC 5304	13:50:01.48	-30:34:42.5	13.62	E+pec:	0.012402	140	$5 \times 3600$	LCO
SN 2005bl	NGC 4070	12:04:11.30	+20:24:35.4	14.06	E	0.024060	170	$2 \times 600$	MMT
SN 2005el	NGC 1819	05:11:46.14	+05:12:02.2	13.69	SB0;Sbrst	0.014910	130	$1 \times 1800, 3 \times 900$	LCO, MMT
SN 2005mc	UGC 04414	08:27:05.96	+21:38:43.0	14.41	S0a	0.025221	120	$3 \times 900$	MMT
SN 2006N	CGCG 308-009	06:08:30.39	+64:43:25.3	14.6	E <sup>b</sup>	0.014277	80	$1 \times 900$	MMT
SN 2006bd	UGC 06609	11:38:29.46	+20:31:39.8	14.72	E	0.025724	100	$2 \times 600 + 2 \times 900$	MMT
SN 2006bq	NGC 6685	18:39:58.64	+39:58:54.4	14.59	S0-:	0.021905	20	$2 \times 600$	MMT
SN 2006cs	CGCG 190-050	13:45:34.99	+35:36:40.1	14.77	S0?	0.023676	34	$2 \times 600$	MMT
SN 2006ef	NGC 0809	02:04:18.97	-08:44:07.1	14.59	(R)S0+:	0.017902	175	$3 \times 3600$	LCO
SN 2006ej	IC 1563	00:39:00.24	-09:00:52.5	14.59	S0pecsp	0.020452	90	$1 \times 1800$	LCO
SN 2006kf	UGC 02829	03:41:50.86	+08:09:35.4	14.94	S0	0.021301	160	$4 \times 1800, 1 \times 900$	LCO, MMT
SN 2006ot	ESO 544-G031	02:15:04.60	-20:46:03.7	15.4	Sa	0.053100	4	$1 \times 3600$	LCO
SN 2007R	MCG +08-14-043	07:46:37.71	+44:47:25.9	14.38	S0/a	0.030880	165	$3 \times 900$	MMT
SN 2007ap	MCG +03-41-003	15:56:23.59	+16:31:23.9	14.65	SA0+	0.015818	40	$2 \times 600$	MMT
SN2007au	UGC 03725	07:11:41.82	+49:52:00.0	14.15	S0-:	0.020584	125	$3 \times 900$	MMT
SN 2007ci	NGC 3873	11:45:46.10	+19:46:26.2	13.85	E	0.018126	0	$2 \times 600$	MMT
SN 2007cp	IC 0807	12:42:12.49	-17:24:12.8	14.6	E-S0 <sup>b</sup>	0.036595	95	$1 \times 3600$	LCO
SN 2007hj	NGC 7461	23:01:48.33	+15:34:56.9	14.48	SB0	0.014113	155	$2 \times 900$	MMT
SN 2007jh	CGCG 391-014	03:36:01.59	+01:06:17.1	15.51	E0	0.040796	55	$3 \times 900$	MMT
SN 2007nq	UGC 00595	00:57:34.92	-01:23:27.9	14.38	E;Radio galaxy;LEG	0.045031	140	$3 \times 3600$	LCO
SN 2008C	UGC 03611	06:57:11.73	+20:26:14.5	15.05	S0/a	0.016621	60	$3 \times 900$	MMT
SN 2008L	NGC 1259	03:17:17.28	+41:23:07.8	15.21	S0	0.019400	100/10	$1 \times 900/1 \times 900$	MMT
SN 2008R	NGC 1200	03:03:54.48	-11:59:30.5	13.8	SA(s)0-	0.013503	130	$3 \times 3600$	LCO
SN 2008af	UGC 09640	14:59:27.64	+16:38:42.4	14.32	E	0.033507	100	$2 \times 600$	MMT

Table 1 *continued on next page*



**Table 1** (*continued*)

SN	Galaxy	R.A.	Decl.	$B^T$	Morphology	$z$	PA	Exposure	Telescope
		(J2000)	(J2000)	(mag)			( $^\circ$ )	( $N \times s$ )	
SN 2008gl	UGC 00881	01:20:53.47	+04:48:04.8	15.26	E	0.034017	40	$3 \times 900$	MMT
SN 2008hv	NGC 2765	09:07:36.64	+03:23:34.5	13.18	S0	0.012549	107	$2 \times 1800 + 5 \times 3600, 4 \times 900$	LCO, MMT
SN 2008ia	ESO 125-G006	08:50:35.85	-61:16:40.5	11.94 <sup>I</sup>	S0	0.021942	35	$6 \times 3600$	LCO
SN 2009F	NGC 1725	04:59:22.89	-11:07:56.3	13.82	S0	0.012956	15	$3 \times 3600$	LCO
SN 2010H	IC 0494	08:06:24.12	+01:02:09.8	14.26	SA0 <sup>+</sup> 0 <sup>-</sup> :	0.015367	45	$3 \times 900$	MMT
SN 2010Y	NGC 3392	10:51:03.00	+65:46:53.6	14.59	E?BLAGN	0.010860	115	$2 \times 900$	MMT

<sup>a</sup>Information from NED and HyperLeda (the total  $B$  magnitude,  $B^T$ ).

<sup>b</sup>Morphological classification is adopted from HyperLeda.

<sup>c</sup>Initially classified as an early-type.

**Table 2.** SALT2 Light-curve Parameters of SNe Ia in Our Sample

SN	Galaxy	$m_B$	Error	$X_1$	Error	$C$	Error	HR	Error
		(mag)						(mag)	
SN 1990af	2MASX J21345926-6244143	17.777	0.032	-2.132	0.141	-0.043	0.044	-0.068	0.167
SN 1992bo	ESO 352-G057	15.782	0.033	-1.98	0.064	-0.045	0.028	0.234	0.109
SN 1993ac	CGCG 307-023	17.777	0.108	-0.896	0.521	0.016	0.042	-0.059	0.204
SN 1993ag	2MASX J10033546-3527410	17.834	0.034	-0.832	0.136	0.057	0.045	-0.176	0.171
SN 1994M	NGC 4493	16.294	0.035	-1.405	0.090	0.055	0.028	-0.186	0.110
SN 1997E	NGC 2258	15.114	0.029	-1.702	0.087	0.016	0.022	0.060	0.087
SN 1997cn	NGC 5490	...	...	...	...	...	...	...	...
SN 1998bp	NGC 6495	15.308	0.034	-2.492	0.092	0.194	0.024	0.06	0.096
SN 1999ej	NGC 0495	15.339	0.052	-1.485	0.223	-0.032	0.031	0.578	0.13
SN 2000dk	NGC 0382	15.364	0.027	-2.047	0.077	-0.023	0.022	-0.06	0.086
SN 2001ie	UGC 05542	16.666	0.042	-0.588	0.119	-0.024	0.027	0.046	0.110
SN 2002G	CGCG 189-024	18.450	0.035	0.197	0.050	-0.046	0.023	-0.265	0.172
SN 2002dj	NGC 5018	13.955	0.033	0.006	0.129	0.063	0.023	-0.478	0.093
SN 2002do	MCG +07-41-001	15.473	0.032	-3.04	0.178	-0.044	0.027	0.146	0.108
SN 2002fb	NGC 0759	...	...	...	...	...	...	...	...
SN 2003ch	UGC 03787	16.675	0.028	-1.347	0.155	-0.039	0.023	0.435	0.092
SN 2003ic	MCG -02-02-086	17.607	0.03	-1.999	0.203	-0.066	0.029	-0.306	0.115
SN 2003iv	UGC 02320 NOTES01	16.973	0.028	-2.157	0.188	-0.095	0.027	0.221	0.107
SN 2004gc	ARP 327NED04	16.721	0.076	-0.682	0.04	0.078	0.022	-0.254	0.111
SN 2004gs	MCG +03-22-020	17.140	0.082	-1.844	0.032	0.121	0.019	0.076	0.108
SN 2005ag	SDSS J145643.21+091936.4	18.450	0.035	0.197	0.050	-0.046	0.023	-0.095	0.092
SN 2005al	NGC 5304	14.865	0.165	-1.220	0.029	-0.096	0.019	0.296	0.179
SN 2005bl	NGC 4070	...	...	...	...	...	...	...	...
SN 2005el	NGC 1819	14.843	0.028	-1.342	0.032	-0.131	0.021	0.151	0.083
SN 2005mc	UGC 04414	17.031	0.089	-1.916	0.044	0.186	0.021	-0.159	0.118
SN 2006N	CGCG 308-009	15.055	0.029	-1.955	0.059	-0.097	0.021	0.221	0.083
SN 2006bd	UGC 06609	...	...	...	...	...	...	...	...
SN 2006bq	NGC 6685	16.193	0.027	-1.568	0.059	0.028	0.022	0.058	0.086
SN 2006cs	CGCG 190-050	...	...	...	...	...	...	...	...
SN 2006ef	NGC 0809	15.443	0.083	-1.092	0.204	-0.094	0.042	0.347	0.178

Table 2 continued on next page

**Table 2** (*continued*)

SN	Galaxy	$m_B$	Error	$X_1$	Error	$C$	Error	HR	Error
		(mag)						(mag)	
SN 2006ej	IC 1563	15.680	0.026	-1.488	0.041	-0.041	0.020	0.061	0.078
SN 2006kf	UGC 02829	15.805	0.107	-1.993	0.054	-0.079	0.020	0.074	0.130
SN 2006ot	ESO 544-G031	17.982	0.047	0.641	0.086	0.093	0.020	-0.037	0.088
SN 2007R	MCG +08-14-043	16.697	0.045	-1.346	0.105	-0.125	0.031	0.336	0.124
SN 2007ap	MCG +03-41-003	15.348	0.041	-1.688	0.069	-0.109	0.029	0.324	0.115
SN 2007au	UGC 03725	16.550	0.033	-3.090	0.116	0.144	0.028	-0.104	0.110
SN 2007ci	NGC 3873	15.895	0.032	-2.827	0.099	0.011	0.027	-0.105	0.106
SN 2007cp	IC 0807	17.133	0.040	-4.011	0.88	-0.052	0.040	-0.319	0.202
SN 2007hj	NGC 7461	15.520	0.035	-2.137	0.063	0.100	0.027	0.157	0.106
SN 2007jh	CGCG 391-014	...	...	...	...	...	...	...	...
SN 2007nq	UGC 00595	17.414	0.054	-1.917	0.051	-0.028	0.02	-0.153	0.092
SN 2008C	UGC 03611	15.644	0.129	-0.719	0.046	0.126	0.019	-0.221	0.147
SN 2008L	NGC 1259	15.097	0.037	-1.592	0.100	-0.151	0.032	-0.097	0.125
SN 2008R	NGC 1200	15.252	0.170	-2.170	0.048	0.047	0.020	0.080	0.185
SN 2008af	UGC 09640	16.857	0.057	-1.425	0.130	-0.031	0.032	-0.061	0.133
SN 2008gl	UGC 00881	16.792	0.03	-1.408	0.098	-0.04	0.028	-0.017	0.109
SN 2008hv	NGC 2765	14.732	0.162	-1.220	0.030	-0.068	0.019	0.011	0.177
SN 2008ia	ESO125-G006	15.841	0.099	-1.312	0.044	-0.039	0.019	-0.118	0.121
SN 2009F	NGC 1725	...	...	...	...	...	...	...	...
SN 2010H	IC 0494	...	...	...	...	...	...	...	...
SN 2010Y	NGC 3392	14.987	0.040	-2.503	0.084	-0.07	0.031	0.487	0.122

**Table 3.** Instrumental Setup for Observations at MMT 6.5-m

Blue Channel Spectrograph	
Grating and Blaze	300 l/mm , 5500 Å
Spectral range	3200-8000 Å
Resolution	$\sim 8 \text{ \AA} / \text{FWHM}$
Dispersion	1.96Å/pixel
Slit width	1".5
Slit length	180"

NOTE—Dates of observations: 2014 May 1-2; 2015 January 15 - 17; 2016 December 22-23, 25-27

**Table 4.** Line Measurements of Our Host Galaxy Sample

SN	Galaxy	$\sigma_v$	Error	H $\beta$	Error	Mg <i>b</i>	Error	Fe5270	Error	Fe5335	Error
		(km/s)		(Å)		(Å)		(Å)		(Å)	
SN 1990af	2MASX J21345926-6244143	191.7	3.3	1.683	0.060	4.255	0.065	3.263	0.148	3.186	0.113
SN 1992bo	ESO 352- G 057	180.3	2.7	1.620	0.038	4.248	0.040	2.945	0.043	3.052	0.051
SN 1993ac	CGCG 307-023	284.1	5.8	1.615	0.033	4.944	0.042	2.861	0.045	2.827	0.068
SN 1993ag	2MASX J10033546-3527410	201.7	2.8	1.604	0.034	3.911	0.036	2.754	0.121	2.709	0.092
SN 1994M	NGC 4493	220.6	2.9	1.744	0.044	5.083	0.048	2.930	0.052	2.850	0.064
SN 1997E	NGC 2258	302.0	9.6	1.566	0.019	5.455	0.022	3.208	0.024	2.870	0.033
SN 1997cn	NGC 5490	356.2	5.1	1.480	0.017	5.464	0.021	3.181	0.023	2.983	0.033
SN 1998bp	NGC 6495	198.3	12.7	1.561	0.037	5.474	0.039	3.018	0.045	2.679	0.056
SN 1999ej	NGC 0495	157.4	15.1	1.966	0.032	4.459	0.035	3.294	0.038	3.086	0.045
SN 2000dk	NGC 0382	196.1	11.9	1.563	0.033	4.535	0.038	3.358	0.042	3.016	0.050
SN 2001ie	UGC 05542	205.5	5.5	1.683	0.060	3.577	0.068	2.951	0.072	2.784	0.086
SN 2002G	CGCG 189-024	142.0	9.4	1.827	0.047	4.978	0.053	2.978	0.059	2.794	0.074
SN 2002dj	NGC5018	215.4	2.4	2.618	0.009	3.229	0.009	2.781	0.010	2.570	0.013
SN 2002do	MCG+07-41-001	288.6	9.0	1.627	0.015	5.282	0.018	3.106	0.020	3.153	0.027
SN 2002fb	NGC 0759	272.0	12.3	2.814	0.026	3.637	0.031	2.648	0.033	2.520	0.043
SN 2003ch	UGC03787	199.6	3.3	2.610	0.052	3.495	0.054	2.605	0.059	2.429	0.072
SN 2003ic	MCG-02-02-086	350.2	5.7	1.380	0.064	5.175	0.077	3.054	0.148	2.582	0.124
SN 2003iv	UGC 02320 NOTES01	206.9	12.1	1.811	0.030	4.417	0.034	3.023	0.039	2.761	0.047
SN 2004gc	ARP327NED04	20.7	64.6	4.710	0.047	2.776	0.051	1.746	0.059	1.796	0.066
SN 2004gs	MCG+03-22-020	115.6	21.3	2.018	0.044	4.039	0.047	2.959	0.051	2.666	0.058
SN 2005ag	2MASX J14564322+0919361	172.7	9.4	4.982	0.104	2.256	0.144	2.017	0.125	1.680	0.144
SN 2005al	NGC5304	222.5	4.4	1.836	0.034	4.476	0.035	2.785	0.039	2.719	0.049
SN 2005bl	NGC4070	175.1	10.8	2.000	0.045	3.955	0.050	2.914	0.054	2.872	0.066
SN 2005el	NGC1819	195.1	7.1	4.548	0.081	2.913	0.082	2.242	0.093	2.032	0.121
SN 2005mc	UGC04414	216.9	11.6	1.454	0.044	4.834	0.047	3.129	0.053	2.768	0.066
SN 2006N	CGCG308-009	167.1	4.5	1.968	0.042	4.373	0.045	2.792	0.051	2.579	0.063
SN 2006bd	UGC06609	211.2	7.9	1.636	0.037	5.168	0.041	2.928	0.046	2.700	0.057
SN 2006bq	NGC6685	175.0	13.1	1.782	0.043	4.951	0.047	2.845	0.053	2.688	0.066
SN 2006cs	CGCG190-050	227.4	6.3	1.841	0.040	4.512	0.045	3.007	0.050	2.644	0.061
SN 2006ef	NGC0809	180.6	3.0	2.014	0.035	4.234	0.036	3.158	0.040	3.168	0.049

Table 4 continued on next page

Table 4 (*continued*)

SN	Galaxy	$\sigma_v$	Error	H $\beta$	Error	Mg <i>b</i>	Error	Fe5270	Error	Fe5335	Error
		(km/s)		(Å)		(Å)		(Å)		(Å)	
SN 2006ej	IC1563	233.1	4.9	1.828	0.140	4.903	0.153	2.562	0.171	2.835	0.221
SN 2006kf	UGC02829	284.1	4.4	1.454	0.029	4.648	0.032	3.017	0.035	3.014	0.046
SN 2006ot	ESO544-G031	286.7	3.9	1.764	0.089	4.681	0.102	3.149	0.114	2.768	0.148
SN 2007R	MCG+08-14-043	211.1	9.4	1.663	0.032	4.360	0.037	2.980	0.042	2.899	0.049
SN 2007ap	MCG+03-41-003	105.9	17.5	2.081	0.044	4.398	0.045	3.144	0.050	2.912	0.057
SN 2007au	UGC03725	290.9	9.5	1.453	0.023	5.766	0.029	3.017	0.032	2.761	0.041
SN 2007ci	NGC3873	244.6	5.0	1.826	0.027	4.678	0.031	2.830	0.035	2.721	0.044
SN 2007cp	IC0807	189.1	4.8	2.232	0.077	4.054	0.080	2.720	0.090	2.562	0.110
SN 2007hj	NGC7461	154.8	4.5	1.632	0.029	4.969	0.031	2.817	0.034	2.610	0.041
SN 2007jh	CGCG391-014	198.4	4.1	1.910	0.035	4.391	0.041	2.990	0.046	2.602	0.060
SN 2007nq	UGC00595	244.4	4.3	1.668	0.073	4.940	0.079	2.851	0.088	2.955	0.160
SN 2008C	UGC03611	74.7	23.9	4.403	0.033	2.791	0.034	2.315	0.038	1.817	0.044
SN 2008L	NGC1259	147.5	5.0	2.197	0.049	4.406	0.053	2.748	0.060	2.400	0.073
SN 2008R	NGC1200	249.8	3.7	1.652	0.031	5.103	0.034	3.239	0.037	3.072	0.048
SN 2008af	UGC09640	218.6	5.8	1.868	0.045	4.725	0.051	3.250	0.056	2.950	0.069
SN 2008gl	UGC00881	177.2	4.3	2.087	0.063	4.689	0.071	2.891	0.079	2.905	0.095
SN 2008hv	NGC2765	190.7	2.5	1.897	0.024	3.989	0.025	2.983	0.028	2.792	0.034
SN 2008ia	ESO125-G006	213.0	2.4	1.920	0.013	4.036	0.014	2.913	0.016	2.731	0.020
SN 2009F	NGC1725	273.8	4.6	1.789	0.028	5.328	0.030	3.096	0.033	3.161	0.043
SN 2010H	IC0494	91.3	5.7	2.771	0.026	3.368	0.029	2.986	0.031	2.778	0.036
SN 2010Y	NGC3392	121.8	5.2	2.089	0.047	4.556	0.049	2.745	0.054	2.437	0.064

**Table 5.** Determined Age and Metallicity of Our Host Galaxy Sample

SN	Galaxy	YEPS		TMJ11		S07	
		Age (Gyr)	[M/H] (dex)	Age (Gyr)	[M/H] (dex)	Age (Gyr)	[M/H] (dex)
SN 1990af	2MASX J21345926-6244143	$5.38^{+1.40}_{-0.78}$	$0.39^{+0.15}_{-0.14}$	$9.20^{+2.12}_{-2.80}$	$0.37^{+0.11}_{-0.13}$	$9.82^{+1.71}_{-1.51}$	$0.15^{+0.09}_{-0.09}$
SN 1992bo	ESO 352-G057	$7.17^{+0.97}_{-0.84}$	$0.21^{+0.06}_{-0.06}$	$11.87^{+1.23}_{-1.11}$	$0.17^{+0.05}_{-0.05}$	$11.80^{+0.88}_{-0.99}$	$0.07^{+0.04}_{-0.05}$
SN 1993ac	CGCG 307-023	$6.65^{+0.83}_{-0.73}$	$0.35^{+0.07}_{-0.06}$	$12.47^{+1.24}_{-1.17}$	$0.22^{+0.06}_{-0.06}$	$11.76^{+0.87}_{-0.83}$	$0.20^{+0.05}_{-0.06}$
SN 1993ag	2MASX J10033546-3527410	$9.28^{+1.20}_{-1.19}$	$-0.03^{+0.11}_{-0.11}$	$12.93^{+1.57}_{-2.29}$	$0.33^{+0.09}_{-0.10}$	$12.92^{+1.37}_{-1.13}$	$-0.07^{+0.09}_{-0.09}$
SN 1994M	NGC 4493	$4.77^{+0.65}_{-0.43}$	$0.51^{+0.08}_{-0.07}$	$8.91^{+1.49}_{-1.68}$	$0.38^{+0.06}_{-0.07}$	$9.11^{+1.07}_{-0.88}$	$0.30^{+0.05}_{-0.05}$
SN 1997E	NGC 5490	$5.69^{+0.32}_{-0.28}$	$0.62^{+0.03}_{-0.03}$	$12.28^{+0.99}_{-0.98}$	$0.38^{+0.03}_{-0.03}$	$11.71^{+0.48}_{-0.46}$	$0.33^{+0.02}_{-0.02}$
SN 1997cn	NGC 2258	$6.80^{+0.40}_{-0.36}$	$0.58^{+0.04}_{-0.04}$	$14.95^{+0.69}_{-1.05}$	$0.34^{+0.03}_{-0.03}$	$13.50^{+0.63}_{-0.60}$	$0.30^{+0.02}_{-0.03}$
SN 1998bp	NGC 6495	$6.37^{+0.72}_{-0.69}$	$0.51^{+0.06}_{-0.06}$	$13.78^{+1.39}_{-1.30}$	$0.26^{+0.06}_{-0.06}$	$12.45^{+1.20}_{-0.89}$	$0.30^{+0.04}_{-0.06}$
SN 1999ej	NGC 0495	$3.46^{+0.21}_{-0.24}$	$0.66^{+0.06}_{-0.06}$	$3.52^{+0.39}_{-0.38}$	$0.55^{+0.05}_{-0.04}$	$5.62^{+0.48}_{-0.40}$	$0.31^{+0.04}_{-0.04}$
SN 2000dk	NGC 0382	$6.68^{+0.86}_{-0.70}$	$0.36^{+0.06}_{-0.06}$	$12.40^{+1.20}_{-1.09}$	$0.26^{+0.05}_{-0.05}$	$12.10^{+0.95}_{-0.87}$	$0.15^{+0.04}_{-0.04}$
SN 2001ie	UGC 05542	$7.78^{+1.44}_{-1.44}$	$0.03^{+0.09}_{-0.10}$	$11.21^{+1.83}_{-1.61}$	$0.01^{+0.08}_{-0.10}$	$11.11^{+1.49}_{-1.39}$	$-0.07^{+0.08}_{-0.08}$
SN 2002G	CGCG 189-024	$4.29^{+0.51}_{-0.44}$	$0.53^{+0.09}_{-0.09}$	$6.95^{+1.78}_{-1.54}$	$0.40^{+0.07}_{-0.07}$	$7.90^{+0.93}_{-0.89}$	$0.30^{+0.05}_{-0.05}$
SN 2002dj	NGC 5018	$2.11^{+0.06}_{-0.04}$	$0.45^{+0.02}_{-0.02}$	$1.79^{+0.01}_{-0.01}$	$0.41^{+0.01}_{-0.01}$	$2.32^{+0.04}_{-0.03}$	$0.23^{+0.02}_{-0.02}$
SN 2002do	MCG +07-41-001	$5.03^{+0.20}_{-0.16}$	$0.63^{+0.03}_{-0.02}$	$9.85^{+0.65}_{-0.54}$	$0.43^{+0.02}_{-0.02}$	$10.42^{+0.39}_{-0.38}$	$0.33^{+0.02}_{-0.02}$
SN 2002fb	NGC 0759	$1.78^{+0.04}_{-0.10}$	$0.58^{+0.08}_{-0.03}$	$1.62^{+0.03}_{-0.03}$	$0.62^{+0.05}_{-0.04}$	$1.92^{+0.09}_{-0.13}$	$0.36^{+0.04}_{-0.04}$
SN 2003ch	UGC 03787	$2.21^{+0.25}_{-0.19}$	$0.39^{+0.09}_{-0.09}$	$1.83^{+0.07}_{-0.06}$	$0.43^{+0.07}_{-0.08}$	$2.44^{+0.18}_{-0.19}$	$0.22^{+0.06}_{-0.06}$
SN 2003ic	MCG-02-02-086	$10.48^{+2.31}_{-2.16}$	$0.27^{+0.15}_{-0.17}$	$19.60^{+2.51}_{-2.75}$	$0.07^{+0.14}_{-0.16}$	$18.01^{+3.60}_{-2.95}$	$0.14^{+0.13}_{-0.12}$
SN 2003iv	PGC 010738	$4.85^{+0.46}_{-0.34}$	$0.35^{+0.06}_{-0.05}$	$7.78^{+0.98}_{-0.91}$	$0.31^{+0.05}_{-0.05}$	$8.37^{+0.62}_{-0.60}$	$0.17^{+0.03}_{-0.03}$
SN 2004gc	ARP 327NED04	$0.10^{+<0.01}_{-<0.01}$	$0.32^{+0.06}_{-0.03}$	$0.64^{+0.01}_{-0.09}$	$0.97^{+0.02}_{-0.09}$	$1.10^{+<0.01}_{-<0.01}$	$-0.08^{+0.04}_{-0.03}$
SN 2004gs	MCG+03-22-020	$3.90^{+0.40}_{-0.28}$	$0.32^{+0.08}_{-0.08}$	$4.65^{+0.70}_{-0.80}$	$0.35^{+0.06}_{-0.07}$	$5.67^{+0.85}_{-0.52}$	$0.16^{+0.05}_{-0.04}$
SN 2005ag	SDSS J145643.21+091936.4	$0.10^{+<0.01}_{-<0.01}$	$0.35^{+0.05}_{-0.03}$	$0.54^{+0.05}_{-0.02}$	$0.52^{+0.37}_{-0.24}$	$1.10^{+<0.01}_{-<0.01}$	$-0.25^{+0.08}_{-0.07}$
SN 2005al	NGC 5304	$5.00^{+0.55}_{-0.40}$	$0.29^{+0.06}_{-0.05}$	$7.86^{+1.00}_{-0.98}$	$0.27^{+0.05}_{-0.05}$	$8.31^{+0.59}_{-0.61}$	$0.18^{+0.04}_{-0.05}$
SN 2005bl	NGC 4070	$3.92^{+0.41}_{-0.28}$	$0.34^{+0.09}_{-0.08}$	$4.69^{+0.74}_{-0.85}$	$0.35^{+0.06}_{-0.07}$	$5.81^{+0.81}_{-0.59}$	$0.16^{+0.05}_{-0.04}$
SN 2005el	NGC 1819	$0.10^{+<0.01}_{-<0.01}$	$0.49^{+0.09}_{-0.03}$	$0.63^{+0.03}_{-0.02}$	$0.99^{+<0.01}_{-<0.01}$	$1.09^{+0.01}_{-0.01}$	$-0.03^{+0.46}_{-0.32}$
SN 2005mc	UGC 04414	$9.13^{+1.26}_{-1.21}$	$0.27^{+0.08}_{-0.07}$	$16.75^{+1.65}_{-1.69}$	$0.15^{+0.07}_{-0.07}$	$15.44^{+1.76}_{-1.51}$	$0.13^{+0.06}_{-0.06}$
SN 2006N	CGCG 308-009	$4.27^{+0.47}_{-0.40}$	$0.31^{+0.08}_{-0.07}$	$5.52^{+0.89}_{-0.80}$	$0.31^{+0.06}_{-0.07}$	$6.67^{+0.63}_{-0.78}$	$0.19^{+0.04}_{-0.06}$
SN 2006bd	UGC 06609	$6.10^{+0.71}_{-0.68}$	$0.43^{+0.06}_{-0.06}$	$11.98^{+1.25}_{-1.14}$	$0.25^{+0.06}_{-0.06}$	$11.32^{+0.86}_{-0.89}$	$0.25^{+0.05}_{-0.06}$
SN 2006bq	NGC 6685	$4.93^{+0.71}_{-0.47}$	$0.41^{+0.08}_{-0.07}$	$8.93^{+1.20}_{-1.54}$	$0.31^{+0.06}_{-0.07}$	$8.91^{+0.95}_{-0.81}$	$0.25^{+0.05}_{-0.07}$
SN 2006cs	CGCG 190-050	$4.73^{+0.57}_{-0.43}$	$0.35^{+0.07}_{-0.07}$	$7.39^{+1.21}_{-1.31}$	$0.31^{+0.06}_{-0.06}$	$8.04^{+0.77}_{-0.75}$	$0.20^{+0.04}_{-0.05}$

Table 5 continued on next page

Table 5 (continued)

SN	Galaxy	YEPS		TMJ11		S07	
		Age	[M/H]	Age	[M/H]	Age	[M/H]
		(Gyr)	(dex)	(Gyr)	(dex)	(Gyr)	(dex)
SN 2006ef	NGC 0809	$3.39^{+0.24}_{-0.27}$	$0.61^{+0.07}_{-0.06}$	$3.34^{+0.42}_{-0.36}$	$0.54^{+0.05}_{-0.05}$	$5.21^{+0.42}_{-0.96}$	$0.28^{+0.03}_{-0.04}$
SN 2006ej	IC 1563	$4.79^{+2.30}_{-1.31}$	$0.39^{+0.24}_{-0.22}$	$8.13^{+4.07}_{-4.12}$	$0.30^{+0.21}_{-0.23}$	$8.40^{+3.04}_{-2.43}$	$0.25^{+0.15}_{-0.22}$
SN 2006kf	UGC 02829	$9.27^{+0.84}_{-0.83}$	$0.24^{+0.05}_{-0.05}$	$16.52^{+1.13}_{-1.13}$	$0.14^{+0.04}_{-0.05}$	$15.40^{+1.13}_{-1.00}$	$0.10^{+0.04}_{-0.04}$
SN 2006ot	ESO 544-G031	$4.83^{+1.58}_{-0.86}$	$0.43^{+0.17}_{-0.16}$	$8.40^{+2.72}_{-3.12}$	$0.36^{+0.13}_{-0.15}$	$8.82^{+2.12}_{-1.78}$	$0.22^{+0.10}_{-0.12}$
SN 2007R	MCG +08-14-043	$6.58^{+0.76}_{-0.67}$	$0.24^{+0.06}_{-0.06}$	$11.01^{+0.99}_{-0.85}$	$0.21^{+0.05}_{-0.05}$	$10.96^{+0.77}_{-0.82}$	$0.11^{+0.04}_{-0.05}$
SN 2007ap	MCG +03-41-003	$3.14^{+0.28}_{-0.25}$	$0.61^{+0.07}_{-0.07}$	$3.04^{+0.49}_{-0.27}$	$0.56^{+0.06}_{-0.06}$	$4.31^{+0.90}_{-0.54}$	$0.31^{+0.05}_{-0.04}$
SN 2007au	UGC 03725	$7.36^{+0.56}_{-0.53}$	$0.56^{+0.05}_{-0.04}$	$16.61^{+0.89}_{-0.92}$	$0.30^{+0.04}_{-0.04}$	$14.74^{+0.79}_{-0.84}$	$0.33^{+0.03}_{-0.04}$
SN 2007ci	NGC 3873	$4.82^{+0.40}_{-0.31}$	$0.37^{+0.05}_{-0.05}$	$7.89^{+0.87}_{-0.81}$	$0.30^{+0.05}_{-0.04}$	$8.34^{+0.50}_{-0.52}$	$0.22^{+0.03}_{-0.04}$
SN 2007ep	IC 0807	$3.12^{+0.52}_{-0.40}$	$0.37^{+0.13}_{-0.14}$	$3.05^{+0.86}_{-0.57}$	$0.40^{+0.10}_{-0.11}$	$3.72^{+1.08}_{-0.52}$	$0.21^{+0.09}_{-0.09}$
SN 2007hj	NGC 7461	$6.91^{+0.64}_{-0.55}$	$0.30^{+0.05}_{-0.04}$	$12.64^{+0.98}_{-0.94}$	$0.16^{+0.04}_{-0.04}$	$11.74^{+0.70}_{-0.67}$	$0.18^{+0.04}_{-0.04}$
SN 2007jh	CGCG 391-014	$4.41^{+0.42}_{-0.37}$	$0.34^{+0.07}_{-0.07}$	$6.03^{+1.02}_{-0.79}$	$0.33^{+0.06}_{-0.06}$	$7.17^{+0.64}_{-0.60}$	$0.19^{+0.04}_{-0.04}$
SN 2007nq	UGC 00595	$5.70^{+1.67}_{-1.10}$	$0.42^{+0.14}_{-0.14}$	$10.90^{+2.54}_{-2.69}$	$0.27^{+0.13}_{-0.13}$	$10.60^{+1.86}_{-1.86}$	$0.23^{+0.09}_{-0.12}$
SN 2008C	UGC 03611	$0.10^{+<0.01}_{-<0.01}$	$0.60^{+0.02}_{-0.02}$	$0.64^{+0.05}_{-0.04}$	$0.99^{+<0.01}_{-0.01}$	$1.10^{+<0.01}_{-<0.01}$	$0.07^{+0.17}_{-0.10}$
SN 2008L	NGC 1259	$3.23^{+0.36}_{-0.32}$	$0.39^{+0.08}_{-0.09}$	$3.30^{+0.62}_{-0.49}$	$0.41^{+0.07}_{-0.07}$	$4.15^{+0.71}_{-0.52}$	$0.26^{+0.04}_{-0.07}$
SN 2008R	NGC 1200	$4.90^{+0.38}_{-0.27}$	$0.61^{+0.06}_{-0.05}$	$9.39^{+1.27}_{-1.18}$	$0.43^{+0.04}_{-0.04}$	$10.03^{+0.77}_{-0.78}$	$0.30^{+0.04}_{-0.04}$
SN 2008af	UGC 09640	$3.88^{+0.37}_{-0.28}$	$0.62^{+0.08}_{-0.08}$	$4.93^{+1.37}_{-1.12}$	$0.50^{+0.07}_{-0.07}$	$6.88^{+0.85}_{-0.65}$	$0.30^{+0.05}_{-0.05}$
SN 2008gl	UGC 00881	$3.11^{+0.46}_{-0.33}$	$0.60^{+0.12}_{-0.10}$	$3.14^{+0.78}_{-0.43}$	$0.55^{+0.10}_{-0.09}$	$4.63^{+0.90}_{-0.93}$	$0.34^{+0.07}_{-0.07}$
SN 2008hv	NGC 2765	$4.62^{+0.28}_{-0.26}$	$0.26^{+0.04}_{-0.04}$	$6.07^{+0.68}_{-0.44}$	$0.28^{+0.04}_{-0.03}$	$7.26^{+0.46}_{-0.42}$	$0.12^{+0.03}_{-0.03}$
SN 2008ia	ESO 125-G006	$4.55^{+0.16}_{-0.15}$	$0.26^{+0.03}_{-0.03}$	$5.88^{+0.30}_{-0.23}$	$0.28^{+0.02}_{-0.02}$	$7.05^{+0.25}_{-0.22}$	$0.13^{+0.02}_{-0.02}$
SN 2009F	NGC 1725	$4.00^{+0.18}_{-0.16}$	$0.76^{+0.05}_{-0.05}$	$5.80^{+1.00}_{-0.94}$	$0.55^{+0.04}_{-0.04}$	$7.69^{+0.53}_{-0.56}$	$0.40^{+0.04}_{-0.03}$
SN 2010H	IC 0494	$1.69^{+0.09}_{-0.17}$	$0.75^{+0.09}_{-0.06}$	$1.62^{+0.02}_{-0.03}$	$0.67^{+0.04}_{-0.03}$	$1.80^{+0.04}_{-<0.01}$	$0.42^{+0.03}_{-0.03}$
SN 2010Y	NGC 3392	$3.65^{+0.36}_{-0.34}$	$0.38^{+0.08}_{-0.09}$	$4.15^{+0.80}_{-0.65}$	$0.38^{+0.06}_{-0.07}$	$5.24^{+0.61}_{-0.54}$	$0.25^{+0.06}_{-0.06}$



**Table 6.** Slope and Significance of the Correlation with Hubble Residual

	Age	log(Age)	[M/H]
Model	( $\Delta\text{mag}/\text{Gyr}$ )	( $\Delta\text{mag}/\text{Gyr}$ )	( $\Delta\text{mag}/\text{dex}$ )
YEPS	$-0.051 \pm 0.022$	$-0.67 \pm 0.26$	$0.29 \pm 0.26$
	98.98% ( $2.3\sigma$ )	99.50% ( $2.6\sigma$ )	86.77% ( $1.1\sigma$ )
TMJ11	$-0.021 \pm 0.007$	$-0.42 \pm 0.14$	$0.70 \pm 0.36$
	99.87% ( $3.0\sigma$ )	99.87% ( $3.0\sigma$ )	97.41% ( $1.9\sigma$ )
S07	$-0.027 \pm 0.010$	$-0.59 \pm 0.21$	$0.45 \pm 0.49$
	99.65% ( $2.7\sigma$ )	99.75% ( $2.8\sigma$ )	82.08% ( $0.9\sigma$ )

**Table 7.** Correlation of SN Ia Brightness with Host Galaxy Property

Host Property	Reference	Original Correlation	Direction	Converted to Age difference
Morphology	Hicken et al. (2009)	$\Delta\text{HR}/\Delta\text{morph.}$	Fainter in	$\sim 0.19$ mag/5.3 Gyr
		$\approx 0.14$ mag/(Scd/Irr - E/S0)	<b>Later type</b> galaxy	Fainter in <b>Younger</b> galaxy
Mass	Sullivan et al. (2010)	$\Delta\text{HR}/\Delta\text{mass}$	Fainter in	$\sim 0.21$ mag/5.3 Gyr
		$\approx 0.08$ mag/( $\Delta\log M_{\star} \sim 1$ )	<b>Less massive</b> galaxy	Fainter in <b>Younger</b> galaxy
Local SFR	Rigault et al. (2018)	$\Delta\text{HR}/\Delta\text{local SFR}$	Fainter in	$\sim 0.34$ mag/5.3 Gyr
		$\approx 0.16$ mag/( $\Delta\log \text{LsSFR}_{\text{step}} \sim 2 \text{ yr}^{-1} \text{ kpc}^{-2}$ )	<b>Higher SFR</b> environments	Fainter in <b>Younger</b> galaxy
Population Age	This work	$\Delta\text{HR}/\Delta\text{age}$	Fainter in	$\sim 0.27$ mag/5.3 Gyr
		$\approx 0.051$ mag/Gyr (YEPS)	<b>Younger</b> galaxy	Fainter in <b>Younger</b> galaxy

This figure "orcid-ID.png" is available in "png" format from:

<http://arxiv.org/ps/1912.04903v1>